Journal of Advanced Ceramics
2019, **8**(1): 19–38
https://doi.org/10.1007/s40145-018-0297-x
ISSN 2226-4108
CN 10-1154/TQ

Review

Recent advances in joining of SiC-based materials (monolithic SiC and SiC_f/SiC composites): Joining processes, joint strength, and interfacial behavior

Guiwu LIU[a,*], Xiangzhao ZHANG[a], Jian YANG[a], Gunjun QIAO[a,b]

[a]*School of Materials Science and Engineering*, *Jiangsu University*, *Zhenjiang 212013*, *China*
[b]*State Key Laboratory for Mechanical Behavior of Materials*, *Xi'an Jiaotong University*, *Xi'an 710049*, *China*

Received: June 29, 2018; Revised: September 8, 2018; Accepted: September 26, 2018

Abstract: Silicon carbide (SiC) has been widely concerned for its excellent overall mechanical and physical properties, such as low density, good thermal-shock behavior, high temperature oxidation resistance, and radiation resistance; as a result, the SiC-based materials have been or are being widely used in most advanced fields involving aerospace, aviation, military, and nuclear power. Joining of SiC-based materials (monolithic SiC and SiC_f/SiC composites) can resolve the problems on poor processing performance and difficulty of fabrication of large-sized and complex-shaped components to a certain extent, which are originated from their high inherent brittleness and low impact toughness. Starting from the introduction to SiC-based materials, joining of ceramics, and joint strength characterization, the joining of SiC-based materials is reviewed by classifying the as-received interlayer materials, involving no interlayer, metallic, glass-ceramic, and organic interlayers. In particular, joining processes (involving joining techniques and parameter conditions), joint strength, interfacial microstructures, and/or reaction products are highlighted for understanding interfacial behavior and for supporting development of application-oriented joining techniques.

Keywords: SiC ceramics; SiC_f/SiC composites; joining; joint strength; interfacial behavior

1 Introduction

Silicon carbide (SiC) is a highly covalent material, containing 88% covalent bond and 12% ionic bond, which makes it own excellent overall properties including high modulus, high stiffness, high melting point, and good wear and corrosion resistances. The SiC-based ceramics are usually fabricated by hot-pressing (HP), hot-isostatic processing (HIP), spark plasma sintering (SPS), pressureless sintering (PLS), liquid-phase sintering (LPS), reaction-bonded (RB) or reaction-formed (RF) process, and chemical vapor deposition (CVD) process, etc. The continuous SiC fiber reinforced SiC ceramic matrix composites (SiC_f/SiC) are a kind of the most important SiC-based materials, which can be mainly prepared by polymer impregnation and pyrolysis (PIP), chemical vapor infiltration (CVI), nano-infiltrated transient eutectoid (NITE), and reaction infiltration (RI) processes [1]. In particular, the SiC_f/SiC composites, which can retain high strength and good high-temperature, oxidation, corrosion, and thermal-shock resistances of SiC ceramics,

* Corresponding author.
E-mail: gwliu76@ujs.edu.cn

are provided with much better service performances than the sintered SiC ceramics, such as good toughness and impact resistances. Therefore, both the SiC ceramics and SiC_f/SiC composites can be used as candidates for high temperature structure–function integrated components in special environments, such as the hot-end components of aerospace engine, thermal protection structure of aerospace craft, and cladding tube of nuclear plant [2].

As we know, joining of ceramics is an issue that we have to face in many practical applications of structural ceramics. Firstly, we need to select the base (ceramic and/or metal) and interlayer materials according to service environment, such as operating temperature and corrosion and radiation level. Secondly, we need to choose an appropriate joining technique based on the shapes of joining components, and bearing stress feature and level. Finally, we have to optimize the joining conditions. In these activities, both the joining technique and joint strength are the two key aspects. Presently, joining techniques of ceramics to themselves or metals mainly involved brazing (including active metal brazing [3], and brazing after surface metallization [4]), diffusion bonding [5], transient liquid phase (TLP) bonding [6], self-propagating high-temperature synthesis (SHS) welding [7], friction welding [8], glass sealing [9], and reaction forming/bonding [10,11], etc. In general, there are respective advantages and disadvantages of each joining technique. For instance, the brazing technique is convenient, flexible, and highly efficient; however, the resulting joints can hardly maintain the strength at elevated temperatures due to the characteristic of relatively low melting point of common brazing alloys. Its demands of diffusion bonding for equipment and joining surface quality of components are very high, and especially joining of large-sized and complex-shaped parts and continuous mass production cannot be carried out effectively although the high-performance joints can be obtained. It is widely believed that the TLP bonding technique has the advantages of both brazing and diffusion bonding to a certain extent, since it belongs to a liquid-based joining process and the high-strength and heat-resistant joints can be also fabricated by the TLP bonding technique. In fact, more or less additional pressure has to be applied on the joining components by the TLP technique, and especially the interfacial behavior is too complicated to control because a series of activities involving interfacial reactions, isothermal solidification, and homogenization of composition need to occur or be completed.

The ceramic/ceramic or ceramic/metal joints are mainly characterized mechanically by shear, bending/flexural and tensile strength. Among all the mechanical features of joints, the shear strength acts as one of the leading properties to assess the reliability of joint. The shear strength can be mainly measured by single lap (SL), single lap offset (SLO), double lap offset (DLO), double-notch (DN), asymmetric 4-point bending (A4PB), torsion square (TS), torsion cylinder (TC), torsion tube (TT) and torsion hourglass (THG), and iosipescu shear (IS) tests [12–14], as shown in Fig. 1. The former four shear tests (SL, SLO, DLO, and DN) are only able to measure the apparent shear strength, while the latter six shear tests (A4PB, TS, TC, TT, THG, and IS) can measure the pure shear strength of ceramic joints. In fact, only the torsional configurations are capable of producing true shear loading and appropriate for testing lap-joined small specimens, and especially the apparent shear strength values determined by the SLO shear test often significantly deviate from the experimental results in a true shear loading state [12,13]. Moreover, the THG test is involved in the torsion drilled hourglass (TDHG) and torsion ring hourglass (TRHG) ones, and a modification of SL test

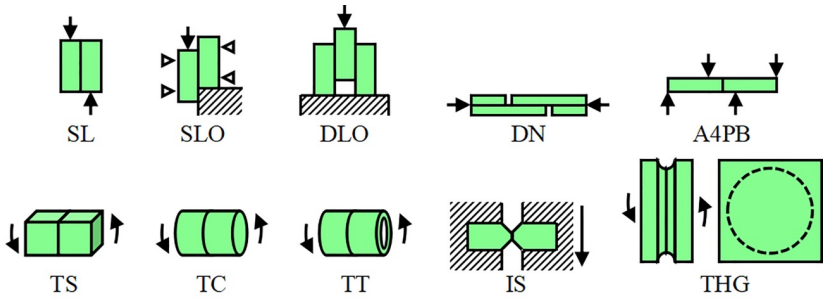

Fig. 1 Methods of shear (and apparent shear) strength evaluation available for ceramic joints. Reproduced with permission from Ref. [12], © Elsevier B.V. 2013; Ref. [13], © The American Ceramic Society 2012; Ref. [14], © The American Ceramic Society 2013.

is usually adopted by applying a direct shear-load at the bonding position of cylinder or square joint [3,4, 15,16]. The bending strength test mainly involves 3-point bending (3PB) and 4-point bending (4PB) modes, and there are three different joint configurations for the 4-point bending [17,18], as shown in Fig. 2. In addition, two kinds of non-standard bonding or shear strength tests were developed by Li's group [19–24], one is that a cylindrical sample of $\varnothing$ = 10 mm was measured by 3-point bending with span of 30 mm, and the other is that the holder fixed the partial metallic part (or ceramic part only for ceramic/ceramic joint) of the welded sample and the load was applied at roughly the middle position of ceramic part (Fig. 3). The joint strengths measured in these two ways are neither a real bending strength, nor a real shear strength, which were called as "joining strength" and "welded strength", respectively.

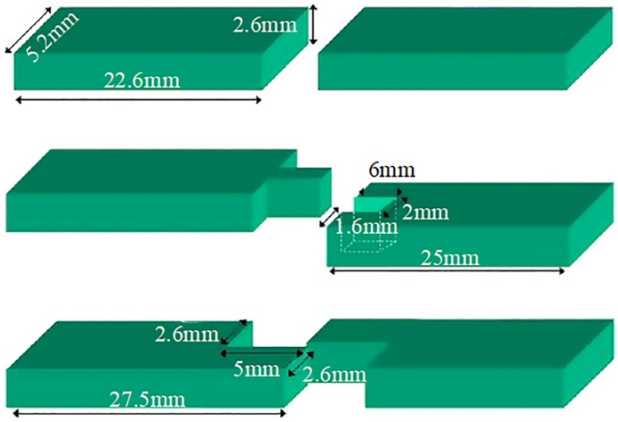

Fig. 2 Three different joint configurations for the 4-point bending test. Reproduced with permission from Ref. [18], © Elsevier B.V. 2008.

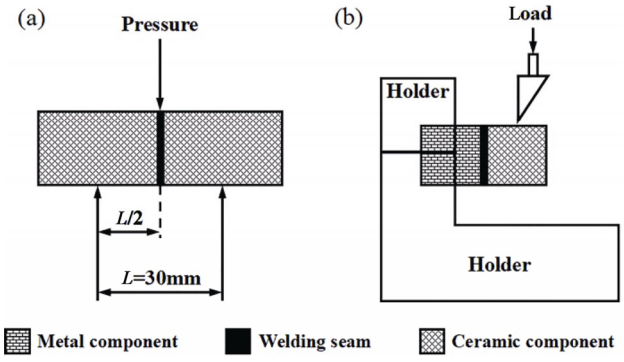

Fig. 3 Schematics of non-standard (a) bonding and (b) shear strength tests for ceramic joints. Reproduced with permission from Ref. [20], © Elsevier B.V. 2010; Ref. [21], © Kluwer Academic Publishers 2003.

To motivate the joining of SiC-based components, we review the joining of monolithic SiC and SiC_f/SiC composites by classifying the as-received interlayer materials, involving no interlayer, metallic, glass-ceramic, and organic materials. The joining techniques and conditions, interfacial microstructures and/or reaction products, as well as joint strength at room and elevated temperatures and under irradiation are highlighted for understanding interfacial behavior and for supporting development of application-oriented joining techniques. What is more, diverse joining techniques and conditions of monolithic SiC and SiC_f/SiC composites can be selected intuitively based on the following collected data according to service demands of joined components.

2 No interlayer

Most of the joining of SiC ceramics and SiC_f/SiC composites to themselves [23,24], graphite [25], and metals (such as W [26–28], F82H steel [29], and Al alloy [30]) using no interlayer was performed by diffusion bonding or hot-pressing sinter bonding process, except that a casting process was adopted to join SiC ceramic to Al alloy, leaving a super-low joint tensile strength of ~0.4 MPa [31,32], as shown in Table 1. The joining temperature varied greatly from 600 to 2000 ℃ with the joining objects while employing the diffusion bonding process, the joining pressure ranged from several to dozens of MPa, and the holding time spanned from 5 to 600 min. Due to more or less difference of coefficient of thermal expansion (CTE) between the SiC-based materials and metals, the resulting ceramic/metal joint strength can change greatly from direct failure for the SiC/F82H steel joint to shear strength of 100 MPa for the SiC/W joint [27,29]. In particular, the diffusion bonding of CVD-SiC ceramic to itself was achieved successfully by spark plasma sintering, and the surface polishing pretreatment presented a huge impact on the joint strength, that is, the average joint 4PB strength increased sharply from 68 to 193 MPa before and after polishing [24]. Moreover, perfect bonding interfaces without visible defects can be observed during diffusion bonding of SiC ceramic plate, disk, and pipe to themselves by spark plasma sintering (Fig. 4); however, the three SiC components were not exactly identical in porosity after diffusion bonding due to two kinds of different preparation processes of SiC ceramics,

Table 1 Joining of SiC-based materials using no interlayer: joining technique, joining conditions, and joint strength

Joining system	Joining technique	Joining conditions	Joint strength characterization	Maximum average joint strength (MPa)	Ref.
SiC/SiC	Diffusion bonding (SPS)	1900 ℃, 30 min, 35 MPa	—	—	[23]
CVD-SiC/CVD-SiC (not polished)	Diffusion bonding (SPS)	2000℃, 5min, 60 MPa	Bending strength (4PB)	68±9	[24]
CVD-SiC/CVD-SiC (polished)	Diffusion bonding (SPS)	1900 ℃, 5 min, 60 MPa	Bending strength (4PB)	193±21	[24]
SiC/graphite	Diffusion bonding (SPS)	1800–2000 ℃, 5 min, 30 MPa	Tensile strength	18	[25]
SiC_f/SiC//W	Diffusion bonding	1600 ℃, 60 min, 20 MPa	Bending strength (3PB)	~125	[26]
PLS-SiC/W	Diffusion bonding Sinter bonding + hot pressing Liquid phase sinter bonding	1500–1800 ℃, 600 min, 20 MPa	Shear strength	100 80 50	[27]
SiC/W	Diffusion bonding	1500 ℃, 30 min, 20 MPa	—	—	[28]
SiC/F82H steel	Diffusion bonding	1000 ℃, 60 min, 10 MPa	Shear strength	Failure	[29]
SiC/Al–0.5Sn(–1Mg)	Diffusion bonding	600 ℃, 60–120 min, 2–8 MPa	Shear strength	51.7 (100 ℃)	[30]
HP-SiC/Al	Casting	700–900 ℃, 10–30 min	Tensile strength	~0.4	[31,32]

Noted that the joint strength values without any temperature and radiation condition denote the ones obtained at or around room temperature, and that the double slash (//) denotes the joining of SiC_f/SiC composites in the whole text.

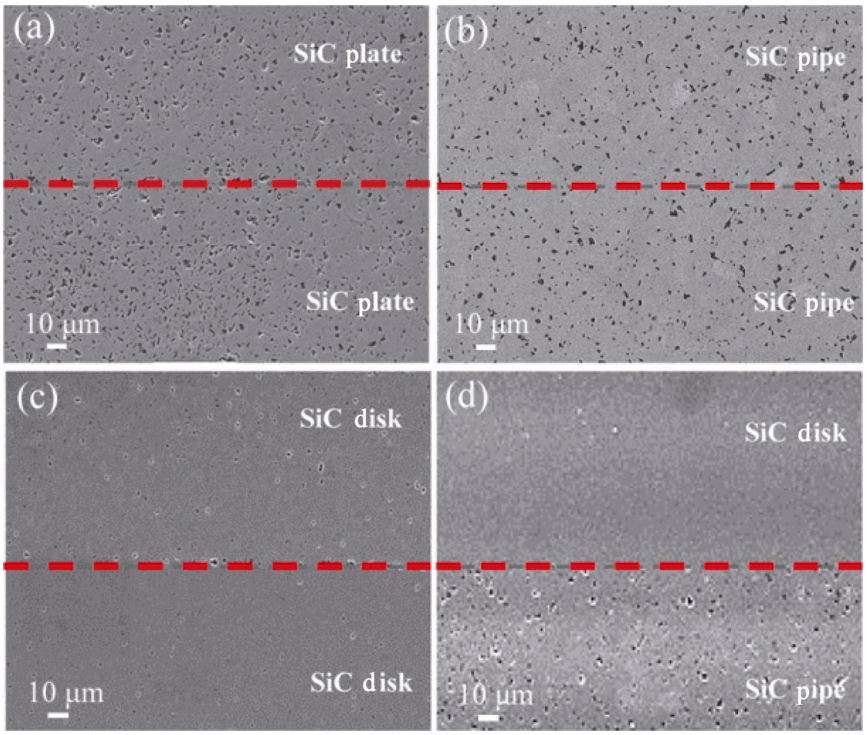

Fig. 4 Cross-sectional SEM images of SiC/SiC joints directly bonded by spark plasma sintering at 1900 ℃, 30 min, 35 MPa: (a) plate couple, (b) pipe couple, (c) disk couple; (d) pipe–disk couple, showing good interfacial bonding and porosity difference in the SiC components. The red dashed lines were located at the bonding interfaces. Reproduced with permission from Ref. [23], © Taylor & Francis 2015.

and the SPS-processed disk-shaped specimens remained almost fully dense [23].

Interfacial reaction and elemental diffusion are the two main bonding mechanisms for direct joining of SiC to metals. The Al_4C_3 was usually formed at the SiC/Al interfaces, and decreasing the formation of Al_4C_3 near the SiC can improve the interfacial bonding due to the presence of alloying elements, such as Sn, Mg, Si [31,32]. Furthermore, only a W-free amorphous reaction layer (which was considered to be non-

equilibrium silicon oxide including carbon) of 500–600 nm thick was detected at the SiC/W interface, and nano-sized precipitates containing O, Si, and W were formed and homogenously distributed in the reaction layer, which can contribute to the interfacial bonding (Fig. 5) [28]. However, in the cases of diffusion bonding, sinter bonding, and liquid phase sinter bonding of PLS-SiC to W, the resulting pores and carbon-rich phases in the reaction layer can deteriorate the joint shear strength although the liquid phase produced during the sintering seemed to facilitate the grain boundary diffusion [27].

3 Metallic interlayer

3. 1 Full metal interlayer

3.1.1 Brazing

The joining techniques of SiC-based materials using metallic materials as interlayer were mainly involved in brazing, diffusion bonding, TLP bonding, and high-temperature rapid combustion reaction welding, etc. The brazing of SiC-based materials can be divided into Ti-containing and Ti-free brazing according to the chemical compositions of brazing fillers.

For the Ti-containing brazing, the brazing fillers were mainly involved in pure Ti [24], Al–Ti [33], Cu–Ti [34,35], Si–Ti [36–38], Ag–Cu–Ti [39–42], Ag–Cu–In–Ti [43–44], Cu–Ag–Ti [44], Cu–Si–Al–Ti [45], Sn–Ag–Ti [46], Ni–Si–Ti [47], and Co–Fe–Ni–(Si,B)–Cr–Ti [48,49] alloys, as shown in Table 2. The brazing temperature varied greatly from 700 ℃ for Ag–Cu–In–Ti to 1700 ℃ for pure Ti with the chemical compositions of brazing fillers, and the holding time ranged from 5 to 60 min. Except the brazing of CVD-SiC to itself by spark plasma sintering [24] and the laser-assisted brazing of SiC to C45E steel [46], any additional pressure does not need to be applied. The SiC/SiC joint strengths at room temperature, regardless of shear and flexural strength, was altered from 50 to 342 MPa, and the maximum average SiC/SiC joint shear and flexural strengths at room temperature were 296 for Al–25Ti and 342 for Ag–35.25Cu–1.75Ti, respectively. Generally, the SiC/SiC joints using the active brazing fillers can present higher joint strength than that using the non- or low reactive brazing filler (such as the Si–16at%Ti). Moreover, the SiC/SiC joints using the two Ag-base brazing fillers (Ag–Cu–Ti and Ag–Cu–In–Ti) only can service at ~500 ℃, and the joint strength can decrease obviously with the testing temperature increasing [41,44]. But, it should be noted that the SiC/SiC joint using the Co-based brazing filler can service over 900 ℃, with 3PB strength of over 180 MPa at 800–900 ℃ [48]. The joint strength of SiC/metal joints ranged from 24.5 to 290 MPa, which was closely related to the CTE of metal components and the chemical composition of brazing fillers.

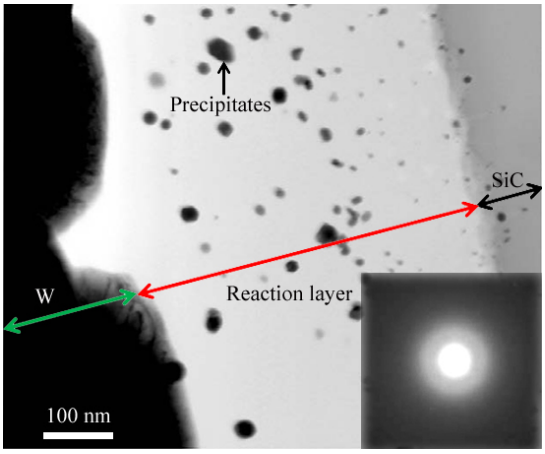

Fig. 5 Interfacial microstructure of diffusion-bonded SiC/W joint. The reaction layer is amorphous and contains Si, O, and C, and the fine precipitates contain O, Si, and W. Reproduced with permission from Ref. [28], © Elsevier B.V. 2011.

The TiC and Ti–Si compounds (Ti_5Si_3 and $TiSi_2$) can usually form at the interlayer/SiC interfaces while employing active Ti-containing brazing fillers. For instance, a continuous TiC layer with grain size of ~10 nm and some discontinuous submicron-scale Ti_5Si_3 grains formed at the Ag–Cu–Ti/SiC interface (Fig. 6(a)) [41], and a couple of nano-sized reaction layers (which were identified as TiC and Ti_5Si_3) can be formed at the Ag–Cu–In–Ti/SiC interface, following an In-containing interfacial layer (Fig. 6(b)) [43]. In fact, the Ti_3SiC_2 or $Ti_3Si(Al)C_2$ MAX phase can also form while using brazing fillers with high concentration of Ti [33–35]. However, the non-reactive phenomenon can be generated while employing the Si–16Ti eutectic alloy and brazing at the eutectic temperature of 1330 ℃ [36]. Moreover, the Cr–C compounds (such as $Cr_{23}C_6$, Cr_3Si, Cr_5Si_3, and $CrSi_2$) and Fe- and Si-containing compounds (Fe_3Si, Fe_2Si, and FeSiC) can be produced due to the presence of Cr and Fe elements derived from the brazing filler (CoFeNi(Si,B)CrTi) or the metal components [42,48].

Table 2 Brazing of SiC-based materials using Ti-containing brazing fillers: interlayer, joining conditions, joint strength, and main phases at interlayer/ceramic interface

Joining system	Interlayer	Joining conditions	Joint strength characterization	Maximum average joint strength (MPa)	Main phases at interlayer/ceramic interface	Ref.
CVD-SiC/CVD-SiC	Ti	1700 ℃, 5 min, 60 MPa (SPS)	Bending strength (4PB)	126±16	TiC_x (Ti–Si, Ti–Si–C: unidentified)	[24]
SiC/SiC	Al–25Ti (at%)	1500 ℃, 10 min (capillary infiltration)	Shear strength (SLO)	296±20	$Ti_3Si(Al)C_2$, Al_3Ti, Al, TiC	[33]
SiC/SiC	Al_3Ti/Ti/Al_3Ti	1500 ℃, 10 min	Shear strength (SLO) Torsion shear strength (THG)	85±9 89±11	$Ti_3Si(Al)C_2$, $(Al,Si)_3Ti$, τ2 Al–Si–Ti	[33]
RBSiC/invar	Cu–75Ti (wt%)	980 ℃, 5–20 min	Shear strength	90	Ti_3SiC_2, TiC, $TiSi_2$	[34]
RBSiC/Ti alloy	Cu–25Ti (wt%)	890–910 ℃, 5–15 min	Shear strength	121.1	$TiSi_2$ or TiSi, CuTiSi, Ti_3SiC_2	[35]
SiC/SiC	Si–16Ti (at%)	1330 ℃, 10–30 min	Shear strength	50	Si, $TiSi_2$	[36]
SiC_f/SiC//SiC_f/SiC	Si–16Ti (at%)	1330 ℃, 10–30 min	Shear strength	71±10; 70 (600 ℃)	Si, $TiSi_2$	[36,37]
SiC/SiC	Si–22Ti (wt%)	1380–1420 ℃, 5–20 min	Shear strength	125	Si, $TiSi_2$, TiC, Ti_5Si_3	[38]
RSiC/WC-Co	Ag–Cu–(0–2.8)Ti (wt%)	800–829 ℃, 0.1 min (laser-assisted)	Shear strength	~57	TiC, Ti_5Si_3, Cu_4Ti	[39]
SiC/TiAl	Ag–27Cu–4.5Ti (wt%)	900 ℃, 5–45 min	Shear strength	~172	Ag–Cu eutectic, Ag(Cu), $Ti(Cu,Al)_2$	[40]
SiC/SiC	Ag–35.25Cu–1.75Ti (wt%)	860–940 ℃, 10–60 min	Bending strength (4PB)	342±69	TiC, Ti_5Si_3	[41]
SiC/SiC	Ag–35.25Cu–1.75Ti (wt%)	900 ℃, 10 min	Bending strength (3PB)	339±29; 155±22 (300 ℃); 139±30 (400℃); 88±29 (500℃)	TiC, Ti_5Si_3	[41]
SiC/SiC; SiC/AISI 304SS; SiC/AISI 3016SS; SiC/Inconel 718	Ag–22.3Cu–1.2Ti (wt%)	930 ℃, 45 min	—	—	TiC, $TiSi_2$, $Cr_{23}C_6$, Cr_5Si_3, $CrSi_2$, FeSiC	[42]
SiC/SiC	Ag–32.25Cu–12.5In–1.25Ti (wt%)	700–800 ℃, 10 min	Bending strength (4PB)	234	TiC, Ti_5Si_3, Ag–Si–In rich phase	[43]
SiC/SiC	Ag–32.25Cu–12.5In–1.25Ti (wt%)	740 ℃, 10 min	Bending strength (4PB)	~257; 230 (300℃); 167 (400℃); 113 (500℃)	TiC, Ti_5Si_3	[44]
SiC/SiC	Ag–32.25Cu–12.5In–1.25Ti (wt%)	740 ℃, 10 min	Torsion shear strength	~183 (450 ℃); 135 (500 ℃); 75 (550 ℃)	TiC, Ti_5Si_3	[44]
SiC/AISI 304SS	Cu–17.25 Ag–4.26Ti (wt%)	930 ℃, 45 min	—	—	TiC, $Cr_{23}C_6$, Cr_5Si_3, Fe_2Si	[42]
SiC/Nb alloy	Cu–3Si–2Al–(0.5–4)Ti (wt%)	1045–1101 ℃, 5 min	Bending strength (3PB)	290 (500 ℃)	TiC, Ti–Si	[45]
PLS-SiC/C45E steel	(30–50)Sn–Ag–2Ti (wt%)	900–950 ℃, 2 min, 2 MPa (laser-assisted)	Shear strength	24.5	—	[46]
SiC/SiC	Ni–Si–(0–10)Ti (wt%)	1450 ℃, 15 min	Bending strength (4PB)	75	—	[47]
HP-SiC/SiC	CoFeNi(Si,B)CrTi	1150–1220 ℃, 5–30 min	Bending strength (4PB)	161	TiC, $Cr_{23}C_6$, Cr_3Si, CoSi, Ni_2Si, Fe_3Si, C	[48]
HP-SiC/SiC	CoFeNi(Si,B)CrTi	1150 ℃, 10 min	Bending strength (3PB)	142.6, 162.3, 188.2, 181.5 (700, 800, 900 ℃)	TiC, $Cr_{23}C_6$, Cr_3Si, CoSi, Ni_2Si, Fe_3Si, C	[48]
HP-SiC/Ni-based superalloy	CoFeNi(Si,B)CrTi+Kovar/W/Ni+CoFeNi (Si,B)CrTi	1150 ℃, 10 min	Bending strength (4PB)	64.6	—	[49]

Recently, two pressureless joining methods of SiC involving *in situ* formation of interfacial $Ti_3Si(Al)C_2$ MAX phase were developed by capillary infiltration of Al_3Ti and using Al_3Ti paste/Ti/Al_3Ti paste interlayer assembly [33]. However, the formation of residual Al and brittle τ_2 phase in Al–Si–Ti system can bring about

poor high temperature resistance and relatively low joint shear strength, respectively. So, to eliminate the formation of low-melting-point and highly brittle intermetallic compound phases by means of thermodynamic calculation can contribute to obtain high strength and high temperature resistant SiC-based ceramic joints, which has both great research value and application prospect.

For the Ti-free brazing, the brazing fillers were mainly involved in low-melting-point Al- [50,51] and Zn-based [52] alloys, and Si- [37,53–55], Co- [56], Ni- [57,58], and PdNi-based [59] high-temperature alloys, as well as $CrSi_2$ intermetallic [54], as shown in Table 3. A novel ultrasonic-assisted brazing was performed to

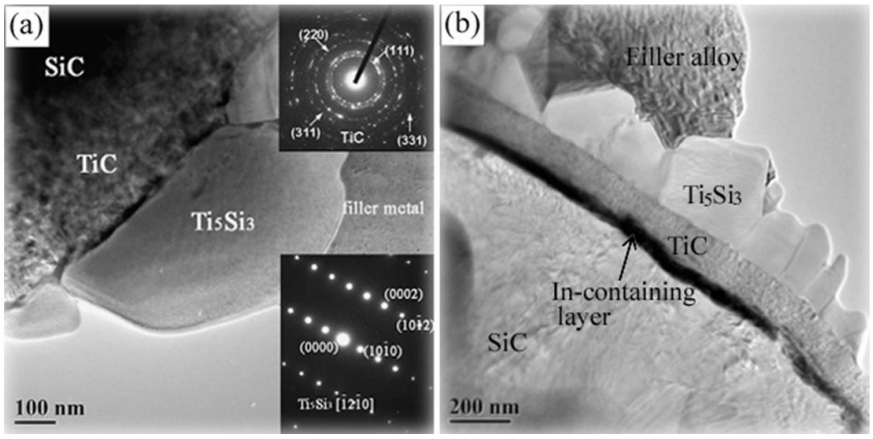

Fig. 6 Interfacial microstructures of SiC/SiC joints brazed using active filler metals of (a) Ag–Cu–Ti and (b) Ag–Cu–In–Ti, showing the presence of TiC and Ti_5Si_3 at the interfaces. Reproduced with permission from Ref. [41], © Elsevier Ltd and Techna Group S.r.l. 2009; Ref. [43], © The Author(s) 2014.

Table 3 Brazing of SiC-based materials using Ti-free brazing fillers: interlayer, joining conditions, joint strength, and main phases at interlayer/ceramic interface

Joining system	Interlayer	Joining conditions	Joint strength characterization	Maximum average joint strength (MPa)	Main phases at interlayer/ceramic interface	Ref.
PLS-SiC/SiC	Al–12Si (wt%)	620 ℃, 2–16 s (ultrasonic-assisted)	Shear strength	94	Al_2SiO_5, Si, amorphous SiO_2	[50]
PLS-SiC/Ti–6Al–4V	Al–12Si (wt%)	620 ℃, 8 s (ultrasonic-assisted)	Shear strength	~22.3	—	[51]
PLS-SiC/Ti–6Al–4V	Al–15.5Sn–9.5Si–4.5Zn–0.5Mg (wt%)	620 ℃, 8 s (ultrasonic-assisted)	Shear strength	~77.8	—	[51]
SiC/SiC	Zn–8.5Al–1Mg (wt%)	420 ℃, 2–16 s (ultrasonic-assisted)	Shear strength	~148.1	Amorphous SiO_2	[52]
SiC/AlN SiC/SiC	Si–17Pr (at%)	1250 ℃, 15 min (capillary infiltration)	—	—	—	[53]
SiC_f/SiC//SiC_f/SiC	Si–44Cr (at%)	1420–1440 ℃, 10 min	Shear strength	66±20	$CrSi_2$, CrSi	[54]
SiC_f/SiC//SiC_f/SiC	$CrSi_2$	1520–1540 ℃, 10 min	Shear strength	64±5	$CrSi_2$	[54]
SiC_f/SiC//SiC_f/SiC	Si–18Cr (at%)	1305 ℃, 10–30min	Shear strength	80±10	$CrSi_2$, Si	[37]
SiC/SiC	Si–18Cr (at%)	1305 ℃, 10–30min	Shear strength	150	$CrSi_2$, Si	[37]
SiC/SiC	Si–29Cr–(0–1)Y (wt%)	1380 ℃, 20 min, 0.01 MPa	Shear strength	88.17	$CrSi_2$, Si	[55]
SiC_f/SiC//SiC_f/SiC	Co–13.5Ni–16.2Nb–10V (wt%)	1280 ℃, 10 min	Bending strength (3PB)	30.8	VC, NbC, Co–Si or (Co,Ni)–Si	[56]
RSiC/RSiC	Ni–51Cr (wt%)	1320–1380 ℃, 1–8 min, 0.05 MPa	3PB strength (circular sample)	74.2	$Cr_{23}C_6$, Cr_7C3, Ni_2Si, C	[57]
SiC/SiC	Ni–49.5Cr–3Nb (wt%)	1380–1420 ℃, 5–10 min	3PB strength (circular sample)	75.1	NbC, Ni_2Si, Cr_5Si_3	[58]
SiC/SiC	PdNi–(16–22)Cr–(7–21) V–Si–B (wt%)	1190–1220 ℃, 10 min	Bending strength (3PB)	84.6	Pd–Si, Ni–Si, Cr(V)–Si, C, $Cr(V)_5Si_3C$, Cr(V)–C	[59]

join SiC to itself in air while employing the two low-melting-point brazing alloys, resulting in the formation of a thin amorphous SiO_2 layer on the SiC ceramic, which can contribute to strong interfacial bonding [50,52]. Moreover, the brazing technique using high-Si alloys (such as Si–17Pr, Si–44Cr, and Si–18Cr) or Si-containing intermetallic ($CrSi_2$) as filler metals can be assigned to the low activation brazing due to the low or non-reactivity between the SiC and these interlayers, in which the direct chemical bonds can be responsible for the interfacial adhesion. However, serious interfacial reactions occurred while employing the Co-, Ni- and PdNi-based high-temperature alloys, leaving a series of brittle reaction products involving (Co, Pd, Ni, Cr)–Si, (Cr, Nb, V)–C, graphite, and $Cr(V)_5Si_3C$, which can bring about relatively low joint bending strength of less than 100 MPa [56–59].

In addition, the SiC_f/SiC joint present higher shear strength than the SiC joint when using Si–16Ti alloy as brazing alloy under same joining conditions [36,37], while the SiC joint had much higher shear strength than the SiC_f/SiC joint when using Si–18Cr alloy as brazing alloy under same joining conditions, with the maximum shear strength of 150 MPa [37]. In this case, the high-strength and high temperature and irradiation resistant joint can be obtained.

3.1.2 Diffusion bonding

The interlayers used for diffusion bonding of SiC-based materials were mainly involved in high-melting-point pure metals (involving Ti [12,60,61] and Mo [62]), metal laminates (such as Ti/Re/Ti [62], Cu/Ti [63], Cu/Ti/M [64], W/Cu [29], W/Ni/Cu/Ni [29], and Zr/Nb [65]) and high-temperature alloys (such as Ti- [5,66,67], Ni- [68–70], W- [71], and Ta-based [72] ones), as shown in Table 4. The applied pressure, joining temperature, and holding time are crucial for diffusion bonding of ceramics, which can affect or determine the formation of reaction products, interfacial microstructure, and joint strength. For instance, the maximum average SiC/SiC joint shear strength using Ti as interlayer climbed obviously from ~6 to 69.6 and 124 MPa with the applied pressure increasing from 0.1 to 7.5 and 20 MPa, respectively [12,60,61]. The Ti_3SiC_2, $Ti_5Si_3C_x$, and/or Ti_2AlC ternary phases can form when the joining temperature was higher than 70% T_m (melting point) of Ti while using Ti or Ti-containing alloys as interlayer [12,61,63,66,67]; however, only the binary compounds (Ti_5Si_3 and TiC) formed while joining at 950–1000 ℃ [60]. At the interlayer (Mo, W, Zr, Ta)/SiC interfaces, the corresponding silicides and carbides can usually form, which was in good accordance with the previous reports and thermodynamic predictions [73]. In particular, the ternary and quaternary brittle compounds ($Ni_5Cr_3Si_2$ and Cr_3Ni_2SiC) can form except Ni–Si and Cr–Si compounds and graphite while using Ni–Cr(–Fe) alloys as interlayer [68–70], which can deteriorate more or less the joint strength. Indeed, the diffusion bonding of SiC-based materials using metallic materials as interlayer can fabricate the high-strength and high temperature and radiation resistant joints, regardless of some technological defects, such as high demands for ceramic surface quality and applied pressure.

Moreover, the microstructural evolution of SiC/Ta–5W interface can be indicated markedly, that is, the thickness of reaction layer increased with the increase of bonding temperature and holding time, and the transverse micro-cracks in the reaction layer seemed to be easier to develop at higher bonding temperature due to the CTE mismatch between phases in the joints (Fig. 7) [72]. For instance, the thickness of reaction layer climbed from 5.13 to 12.71 μm with the holding time increasing from 5 to 30 min at 1500 ℃, and it was raised from 12.72 to 22.85 μm with the temperature increasing from 1500 to 1700 ℃ for 30 min.

In addition, by comparison with the brazing and diffusion bonding of CVD-SiC to itself using Ti as interlayer [12,24], only a titanium-carbon rich phase formed in the joined region with a limited Ti/Si interdiffusion while brazing at 1700 ℃ under 60 MPa for 5 min; however, the original Ti filler was completely conversed into a compound layer involving Ti_3SiC_2 and $Ti5Si_3$ and transverse cracks formed in the bonding layer while diffusion bonding at 1170 ℃ under 20 MPa for 180 min. As a result, the similar joint strength of ~125 MPa, regardless of 4PB and THG shear strength, can be obtained, which can demonstrate the equivalence among the joining parameters (temperature, holding time, and applied pressure) to a certain extent.

3.1.3 Other joining techniques

The TLP bonding, composite joining (brazing+TLP bonding), hot pressing reaction welding, SHS welding or high-temperature rapid combustion reaction welding, and joining method of “higher-temperature wrapping-of-lower-temperature-metals” were developed for joining of SiC-based materials to themselves or metals using

Table 4 Diffusion bonding of SiC-based materials using metallic materials as interlayer: interlayer, joining conditions, joint strength, and main phases at interlayer/ceramic interface

Joining system	Interlayer	Joining conditions	Joint strength characterization	Maximum joint strength (MPa)	Main phases at interlayer/ceramic interface	Ref.
CVD-SiC/CVD-SiC	Ti	1170 ℃, 180 min, 20 MPa	Torsion shear strength	124±23; 125±36 (50℃, 3.4 dpa)	Ti_3SiC_2, Ti_5Si_3	[12]
PLS-SiC/PLS-SiC	Ti	950–1000 ℃, 90–120 min, 7.5 MPa	Shear strength	69.6	Ti_5Si_3, TiC	[60]
SiC/SiC RB-SiC/RB-SiC SSiC/SSiC	Ti foil + Si Ti foil	1480 ℃, 60 min, 0.1 MPa 1450–1510 ℃, 60 min, 0.1 MPa	Torsion shear strength (THG)	100 ~35 ~6	$TiSi_2$, Ti_3SiC_2, SiC	[61]
CVD-SiC/CVD-SiC	Mo	1500 ℃, 600 min, 17.2 MPa	Bending strength (4PB); shear strength (DN)	183±83; 258±157 (1090 ℃) 161.4± 75.3;144.2±67.8 (1090 ℃)	Mo_5Si_3, Mo_2C, C, (Mo_5Si_3+C)	[62]
SiC/SiC	Ti/Re/Ti	1400–1600 ℃, 120 min, 25 MPa	—	—	Ti_3SiC_2, $Ti_5Si_3C_x$, TiC	[63]
SiC_f/SiC//Cu	Cu/Ti Cu/Ti/Mo	1000 ℃, 15–30 min, 0.007 MPa	Shear strength	50–76	—	[64]
PLS-SiC/F82H steel	W/Cu	SiC/W: 1600 ℃, 60 min, 20 MPa; SiC/W/Cu: 1000 ℃, 60 min; SiC/W/Cu/F82H steel: 800–900 ℃, 60 min, 10 MPa	Shear strength	~10	WC, W_5Si_3	[29]
PLS-SiC/F82H steel	W/Ni/Cu/Ni	SiC/W: 1600 ℃, 60 min, 20 MPa; SiC/W/Ni/Cu/Ni/F82H steel: 850–950 ℃, 60 min, 10 MPa	Shear strength	25.6	WC, W_5Si_3	[29]
RSiC/Ni-based alloy	Zr/Nb	1020–1170 ℃, 15–50 min, 6.35–18.7 MPa	Welded strength	46.8	$ZrSi_2$, ZrC	[65]
PLS-SiC/PLS-SiC	Ti–48Al (at%)	1300–1400 ℃, 15–540 min, 125 MPa	—	—	TiC, Ti_2AlC, $Ti_5Si_3C_x$	[66]
SiC/SiC	Ti–43Al–1.7Cr–1.7Nb (at%)	1200–1300 ℃, 15–240 min, 35 MPa	Bending strength (3PB)	240	TiC, $Ti_5Si_3C_x$	[5,67]
SiC/SiC	Ni–25Cr (at%)	1000 ℃, 30–120 min, 7.2 MPa	—	—	Ni_2Si, $Ni_5Cr_3Si_2$, Cr_3Ni_2SiC, C	[68]
RB-SiC/RB-SiC	Ni–25Cr (at%)	950–1050 ℃, 15–60 min, 7.2 MPa	—	—	Ni_2Si, $Ni_5Cr_3Si_2$, Cr_3Ni_2SiC, C	[69]
RB-SiC/RB-SiC	Ni–15.5%Cr–8%Fe (wt%)	900–1080 ℃, 30 min, 2.2 MPa	Shear strength	126	$Ni_5Cr_3Si_2$, $CrSi_2$, Cr_3Si, Ni_2Si, NiSi, C	[70]
SiC/stainless steel	W–1.8Pd–1.2Ni (wt%)	1250–1350 ℃, 30–120 min, 20 MPa	Shear strength	~33	Pd_2Si, Ni_2Si, C, W_5Si_3,WC	[71]
PLS-SiC/PLS-SiC	Ta–5W	1500–1700 ℃, 5–30 min, 2.2 MPa (SPS)	Shear strength	122±15	(Ta,W)C, $(Ta,W)_5Si_3$, $(Ta,W)Si_2$	[72]

metallic interlayers involving Pb [74], Ni–Si/Mo [75], Ti/Ag/Ti [76], Ni–Ti–Al [7,77] and Ti [78], and Mo/Si [79], respectively. However, these joining techniques usually required more or less applied pressure except the "Mo-wrap Si" method [79]. For instance, Liu *et al.* [75] investigated the composite joining of HIP-SiC to Kovar using Ni–Si/Mo (i.e., Ni–56Si powder coated Mo foil) as interlayer at 1350 ℃ for 10 min under a very low applied pressure of ~1 kPa, and obtained two totally different (non-reactive and reactive) interfacial microstructures at the interlayer/SiC and interlayer/Kovar interfaces (Fig. 8) and found that the joint fractured in the SiC near the interface. So, it is quite necessary for joining of SiC-based materials to apply these "new" joining techniques, which indeed possess obvious respective technological advantages. For instance, the TLP bonding can combine advantages of active metal brazing and diffusion bonding, and fabricate high-strength and heat-resistant joints for joining of oxide and non-oxide ceramics.

3. 2 Metal-ceramic hybrid interlayer

To reduce the thermal stress in joint, some low CTE ceramic particles or fibers, such as B_4C, TiC, SiC, and SiO_2, were directly added into Ag–Cu–Ti or Ni–Cr alloys to form composite fillers for brazing of SiC ceramics [80–85], as shown in Table 5. Meanwhile, these low CTE ceramic particles (including SiC, B_4C,

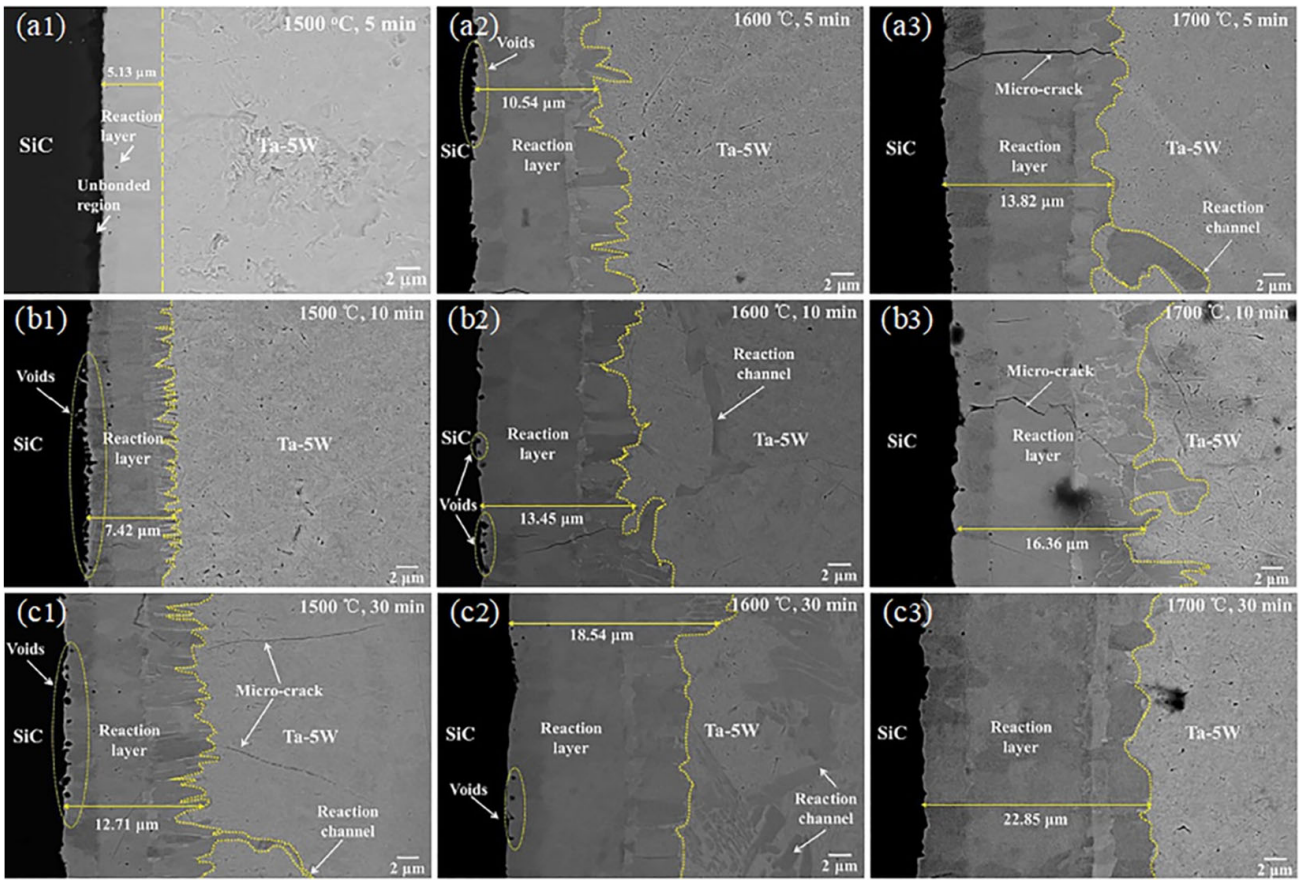

Fig. 7 BSE micrographs of SiC/Ta–5W interface in the SiC/SiC joints diffusion-bonded at (a1–c1) 1500 ℃, (a2–c2) 1600 ℃, and (a3–c3) 1700 ℃ for 5, 10, and 30 min, respectively, showing the interfacial microstructural evolution. Reproduced with permission from Ref. [72], © Elsevier Ltd and Techna Group S.r.l. 2017.

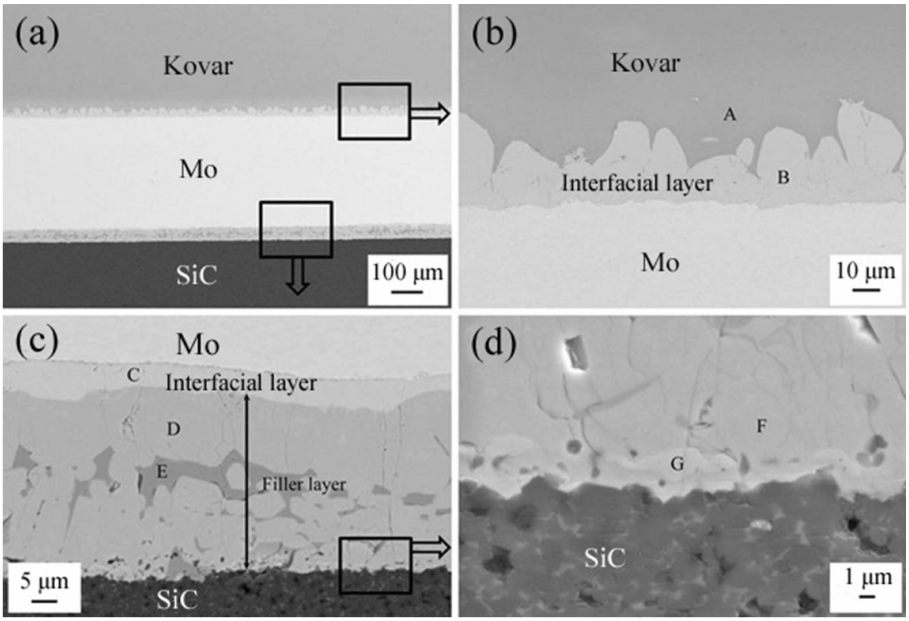

Fig. 8 Cross-sectional and interfacial microstructures of SiC/Kovar joints fabricated by composite joining (brazing+TLP bonding) method using Ni–Si/Mo interlayer: (a) Kovar/SiC joint, (b) Kovar/Mo interface, (c) Mo/Ni–Si/SiC section, (d) Ni–Si/SiC interface. Reproduced with permission from Ref. [75], © Springer Science+Business Media, LLC 2010.

TiC, and C, etc.) combined with metals (such as Al, Ti, Si, and their combinations) acted as interlayers to join SiC ceramics by hot-pressing sinter joining [86], hot-pressing reaction joining [87], Al infiltration [88], and SHS welding [21,78,89] processes. These SiC/SiC joints possessed the relatively high joint strength of 140–530 MPa except the CVD-SiC/CVD-SiC joint fabricated by the microwave assisted combustion synthesis process. As expected, the relatively low joint strength of 10–84 MPa can be obtained between SiC ceramics to metals or graphite (Table 5). Noted that the microwave assisted combustion synthesis process was deemed to a kind of rapid, almost pressureless, and localized heating joining method in spite of the low joint strength, and the resulting joints can be high-temperature and irradiation resistant [89].

4 Glass-ceramic interlayer

Presently, the joining of SiC-based materials using inorganic non-metallic materials as interlayer can only aim at homogeneous materials joining, rather than at dissimilar materials joining. These inorganic non-metallic (glass-ceramic) materials can be divided into three categories: glass ceramic, glass+ceramic, and ceramic. Recently, the glass ceramics were mainly involved in $CaO–Al_2O_3$ (CA) [12,90–93], $Y_2O_3–Al_2O_3–SiO_2$ (YAS) [18,94–99], $Nd_2O_3–Al_2O_3–SiO_2$ [100], $RE_2O_3–Al_2O_3–SiO_2$ (RE = Sc, Yb, Ho, Dy, Y, Nd) [101], $MgO–Al_2O_3–SiO_2$ [97], $Na_2O–B_2O_3–SiO_2$ [102–104] systems, among which the CA and YAS were the most frequently used glass ceramic systems. Here, this joining method using glass ceramics as interlayer can be called as glass-ceramic joining, which can be performed by pressureless or low-pressure process, as shown in Table 6. In particular, a laser-assisted joining process for brazing of SiC capsule specimens using YAS filler can be well performed (Fig. 9). By comparison with the CVD-SiC joint strengths using CA as interlayer, the SLO shear strength was only ~40 MPa, while the average THG shear strength arrived at ~100 MPa [12,91–93]. Moreover, the 4PB strengths of SiC and SiC_f/SiC joint fluctuated in the range of 94.5–236 MP while using YAS as interlayer except a minimum shear strength [18,94–99].

Up to now, the glass+ceramic fillers for joining of SiC-based materials only included SiC+YAS and $SiC+Y_2O_3–Al_2O_3$ (YA) systems (Table 7), in which the SiC was the joining agent and the YAS and YA seemed to act as liquid phase for sintering of SiC ceramic. So, this corresponding joining process was called as transient eutectic-phase (TEP) joining, and this TEP

Table 5 Joining of SiC-based materials using metal-ceramic hybrid materials as interlayer: interlayer, joining conditions, and joint strength

Joining system	Interlayer	Joining conditions	Joint strength characterization	Maximum average joint strength (MPa)	Ref.
RSiC/TC4	Ag–Cu–Ti+(Ti+C)	890–920 ℃, 10–30 min	—	—	[80]
PLS-SiC/PLS-SiC	Ag–Cu–TiH_2+B_4C	850–1000 ℃, 10 min, 0.015 MPa	Bending strength (4PB)	140	[81]
PLS-SiC/PLS-SiC	Ag–Cu–TiH_2+B_4C	950 ℃, 5–15 min, 0.015 MPa	Bending strength (4PB)	140	[82]
SiC/Nb	Ag–Cu–Ti/3D-SiO_2 fiber/Ag–Cu–Ti	970 ℃, 20 min	Shear strength	10	[83]
SiC/Nb	Ti/Ag–Cu–Ti/3D-SiO_2 fiber/Ag–Cu–Ti	970 ℃, 20 min	Shear strength	~45	[83]
SiC/SiC	Ag–Cu–Ti/SiC_P+ Ag–Cu–Ti/Ag–Cu–Ti	900 ℃, 10 min	Bending strength (3PB)	~315; 197 (600 ℃)	[84]
RSiC/graphite	Ni–Cr–SiC	1320–1380 ℃, 3–8 min, 0.05 MPa	Bending strength (3PB)	39.5	[85]
SiC/SiC	SiC+Al–B–C SiC+Al–B_4C–C	1650–1800 ℃, 30 min, 12.5–50 MPa	Bending strength (4PB)	530; 364 ±24	[86]
SiC/SiC	Ti–BN–Al Ti–B_4C–Si	1800 ℃, 60 min, 15 MPa	Bending strength (4PB)	65±19; 142±44	[87]
SiC/SiC	Al+TiC	900–1100 ℃, 30–120 min	Bending strength (3PB)	240	[88]
RSiC/Ni-based alloy	W–Ti–Ni–C/W/W–Ti–Ni–C+TiC–Ni FGM	1190 ℃, 10 min, 25.5 MPa	Welded strength	~84	[21]
SiC/Al alloy	Ti+C powder	High-temperature rapid combustion reaction	—	—	[78]
CVD-SiC/CVD-SiC	Ti+Si+C powder	Microwave assisted combustion synthesis	Shear strength	45.1	[89]

Table 6 Joining of SiC-based materials using glass ceramics as interlayer: interlayer, joining conditions/technique, and joint strength

Joining system	Interlayer	Joining conditions/technique	Joint strength characterization	Maximum average joint strength (MPa)	Ref.
SiC_f/SiC//SiC_f/SiC	$CaO–Al_2O_3$	1500 ℃, 60 min	Shear strength	28	[90]
CVD-SiC/CVD-SiC	$CaO–Al_2O_3$	1480 ℃, 60 min	Shear strength (SLO)	41±6	[91]
CVD-SiC/CVD-SiC	$CaO–Al_2O_3$	1480 ℃, 10 min	Torsional shear strength (THG)	104±25	[92]
CVD-SiC/CVD-SiC	$CaO–Al_2O_3$	1480 ℃, 10 min	Shear strength (SLO)	36±8	[92]
CVD-SiC/CVD-SiC	$CaO–Al_2O_3$	1480 ℃, 10 min	Torsion shear strength (THG)	~100	[93]
CVD-SiC/CVD-SiC	$CaO–Al_2O_3$	1480 ℃,10 min	Torsion shear strength (THG)	115±20; 93±5 (500 ℃, 3.0 dpa); 93±6 (800℃, 5.0 dpa)	[12]
SiC/SiC	$Y_2O_3–Al_2O_3–SiO_2$	Laser brazing	Bending strength (4PB)	236	[94]
SiC/SiC	$Y_2O_3–Al_2O_3–SiO_2$	Laser brazing	Bending strength (4PB)	112±52	[95]
SiC_f/SiC//SiC_f/SiC	$Y_2O_3–Al_2O_3–SiO_2$	1375 ℃, 20 min + 1235 ℃, 60min	Bending strength (4PB)	149	[18]
SiC_f/SiC//SiC_f/SiC	$Y_2O_3–Al_2O_3–SiO_2$	1375 ℃, 20 min + 1235 ℃, 60 min	Bending strength (4PB, type 2) Bending strength (4PB, type 3)	122±10; 118 (600 ℃, 2.6–3.3 dpa); 89 (820 ℃, 5 dpa) 149; 65 (600 ℃, 2.6–3.3 dpa)	[96]
SiC/SiC	$Y_2O_3–Al_2O_3–SiO_2$	Laser joining	Bending strength (4PB)	94.5±13.0; 67.0±5.3 (850 ℃)	[97]
SiC/SiC	$Y_2O_3–Al_2O_3–SiO_2$	Laser joining	—	—	[98]
SiC_f/SiC//SiC_f/SiC	$Y_2O_3–Al_2O_3–SiO_2$	1300–1400 ℃, 0–60 min	Shear strength	39.95	[99]
SiC/SiC	$Nd_2O_3–Al_2O_3–SiO_2$	1346–1564 ℃, ~1.2 min (laser brazing)	Bending strength (4PB)	~150	[100]
SiC/SiC	$RE_2O_3–Al_2O_3–SiO_2$ (RE = Sc, Yb, Ho, Dy, Y, Nd)	1347–1652 ℃, ~1.2 min (laser joining)	Bending strength (4PB)	149	[101]
SiC/SiC	$MgO–Al_2O_3–SiO_2$	Laser joining	Bending strength (4PB)	121.7±28.5; 114.5± 29.5 (850 ℃)	[97]
PLS-SiC/PLS-SiC	$Na_2O–B_2O_3–SiO_2$	1150 ℃, 10 min, ~133 Pa	—	—	[102]
SiC/SiC	$Na_2O–B_2O_3–SiO_2$	1050–1200 ℃, 10–180 min	Bending strength (4PB)	219±19; 154±35 (400 ℃); 111±20 (550 ℃)	[103]
SiC/SiC	$Na_2O–B_2O_3–SiO_2$	1150 ℃, 10 min, 133 Pa	Bending strength (4PB)	~218	[104]

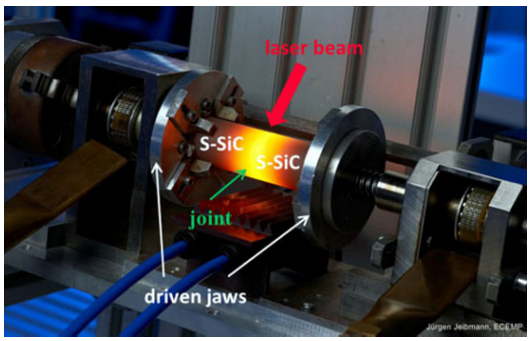

Fig. 9 Laser joining of sintered SiC capsule specimens. Reproduced with permission from Ref. [97], © Taylor & Francis 2015.

joining can be divided into TEPs and TEPt joining while using mixed powder slurry and green tape, respectively [12]. As expected, this TEP joining process was usually conditioned by high temperature and high applied pressure due to the presence of high-volume fraction SiC particles, resulting in relatively high joint strength of ~120–359 MPa.

The ceramic fillers for joining of SiC-based materials were mainly involved in Ti_3SiC_2, Ti_3SiC_2+SiC, Ti_3SiC_2+TiC, SiC+C, TiB_2+C, Y_2O_3 partially stabilized ZrO_2 (YSZ), and YSZ+Al_2O_3, as well as carbonaceous mixture containing Si and SiO_2, as shown in Table 8. While employing the Ti_3SiC_2, SiC, TiB_2, and YSZ as interlayers, the pressurized (hot-pressing sinter/reaction) joining process must be adopted with high applied pressure of 20–50 MPa. However, a pressureless joining process was developed while employing the carbonaceous mixtures as interlayers plus subsequent Si infiltration, which was called as reaction forming/bonding. The joint strengths ranging from tens to hundreds of MPa were obtained due to the great differences of

base and interlayer materials, joining conditions and joint strength characterization method (Table 8), but all these joints can be high-temperature resistant. For instance, the joint room-temperature strength varied from 39.5 to 220.3 MPa with the type of SiC ceramic and testing method of shear strength while using Ti_3SiC_2 as interlayer [20,22,109–111]. In particular, the resulting CVD-SiC joints by SPS joining using Ti_3SiC_2 foil as interlayer possessed average 4PB strength of ~220 MPa at room temperature; however, the initial bending strength did not deteriorate when tested at 1000 ℃ in vacuum, and then linearly decreased to ~20 MPa with the temperature further increasing to 1400 ℃ [111], as shown in Fig. 10.

In short, this kind of joining process using glass-ceramic materials as interlayer belongs to low-activation

Table 7 Joining of SiC-based components using glass+ceramic as interlayer: interlayer, joining conditions, and joint strength

Joining system	Interlayer	Joining conditions	Joint strength characterization	Maximum average joint strength (MPa)	Ref.
SiC/SiC	SiC+Y_2O_3–Al_2O_3–SiO_2	1400–1900 ℃, 20 MPa	Tensile strength Shear strength (A4PB) Torsion shear strength (THG)	249 115 200–250	[91]
SiC/SiC	SiC+Y_2O_3–Al_2O_3–SiO_2	1500–1900 ℃, 60 min, 5–20MPa	Tensile strength	~312	[105]
SiC/SiC	SiC+Y_2O_3–Al_2O_3–SiO_2	1800 ℃, 60 min, 20 MPa	Torsion shear strength (THG)	~214	[106]
SiC/SiC	SiC+Y_2O_3–Al_2O_3–SiO_2	1400–1900 ℃, 20 MPa	Shear strength (A4PB)	120	[107]
CVD-SiC/CVD-SiC NLS-SiC/NLS-SiC NITE-SiC/NITE-SiC	SiC+Y_2O_3–Al_2O_3–SiO_2	1900 ℃, 60 min, 20 MPa	Torsion shear strength (THG)	150±64; 251±40 (500 ℃, 3.0–3.4 dpa) 335±16; 349±38 (500 ℃, 3.4 dpa) 209±14; 182±21 (500 ℃, 3.4 dpa)	[12]
CVD-SiC/CVD-SiC	SiC+Y_2O_3–Al_2O_3	1850 ℃, 60 min, 10 MPa	Torsion shear strength (THG)	150±16; 139±20 (500 ℃, 3.0 dpa) ; 133±13 (800 ℃, 5.0 dpa)	[12]
NLS-SiC/NLS-SiC	SiC+Y_2O_3–Al_2O_3	1850 ℃, 60 min, 10 MPa	Torsion shear strength (THG)	172±4; 126±16 (500 ℃, 3.0 dpa); 143±10 (800 ℃, 5.0 dpa)	[12]
SiC/SiC	SiC+Y_2O_3–Al_2O_3	1800–1900 ℃, 60 min, 15 MPa	Bending strength	359	[108]

Table 8 Joining of SiC-based materials using ceramics as interlayer: interlayer, joining conditions, and joint strength

Joining system	Interlayer	Joining conditions	Joint strength characterization	Maximum average joint strength (MPa)	Ref.
PLS-SiC/PLS-SiC	Ti_3SiC_2	1300–1600 ℃, 30 min, 20–40 MPa	Joining strength	110.4	[20]
RBSiC/RBSiC	Ti_3SiC_2	1300–1500 ℃, 30–90 min, 20–40MPa	Welded strength (3PB)	39.5	[22]
SiC/SiC	Ti_3SiC_2	1250–1600 ℃, 30 MPa (SPS)	Bending strength (3PB)	66; 21 (500 ℃)	[109]
PLS-SiC/PLS-SiC	Ti_3SiC_2	1300–1600 ℃, 5 min, 50 MPa	Bending strength (4PB)	99.1	[110]
CVD-SiC/CVD-SiC	Ti_3SiC_2	1300 ℃, 5 min, 50 MPa (SPS)	Bending strength (4PB)	220.3±3.2 246.3±43 (1000 ℃)	[111]
SiC/SiC SiC_f/SiC//SiC_f/SiC	TiC+Si (3:2) (Ti_3SiC_2+SiC)	1300–1450 ℃, 120 min, 30 MPa	—	—	[112]
CVD-SiC/CVD-SiC	TiC+Si (3:2) (Ti_3SiC_2+SiC)	1425 ℃, 120 min, 30–40 MPa	Torsion shear strength (THG)	117±10 98±22 (800 ℃, 5.0 dpa)	[12]
SiC/SiC	TiC–Si (Ti_3SiC_2+SiC)	1200–1400 ℃, 60 min, 30 MPa	Shear strength (DN)	50	[113]
SiC/SiC	3Ti/1.2Si/2C/0.2Al (Ti_3SiC_2+TiC)	1200–1600 ℃, 30 MPa (SPS)	Bending strength (3PB)	133; 80 (500 ℃); 68 (800 ℃); 119 (1200℃)	[109]
SiC/SiC	4.5YSZ YSZ+Al_2O_3	1600–1800 ℃, 40 MPa (SPS)	Joining strength (3PB)	26.7 107.3	[114]
SiC/SiC	SiC+C	> 1450 ℃ (Si infiltration)	Bending strength (3PB)	~300	[115]
SiC/SiC	TiB_2+C	1450 ℃, 60 min (Si infiltration)	Bending strength (3PB)	422±52	[116]
RFSiC/RFSiC	Carbonaceous mixture (C+Si+SiO_2)	1500–1900 ℃ (Si infiltration)	Bending strength (3PB)	461.8	[117]
RFSiC/RFSiC	Carbonaceous mixture (C+Si+SiO_2)	1600 ℃, 15 min (Si infiltration)	Bending strength (3PB)	465	[118]
SiC_f/SiC//SiC_f/SiC SiC_f/SiC//SiC_f/SiC SiC/SiC	Carbonaceous mixture	1425 ℃, 5–10 min (Si infiltration)	Shear strength (A4PB) Bending strength (4PB)	28±7 78.8±8 255±3.2	[119]

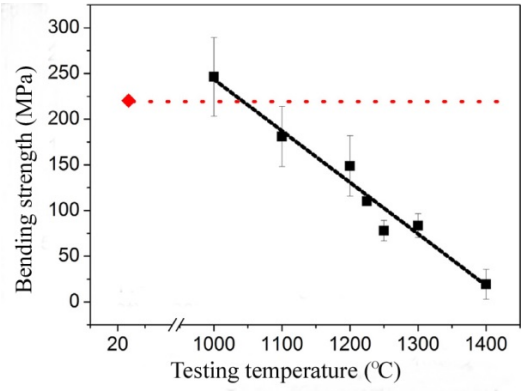

Fig. 10 4-Point bending strength of CVD-SiC/CVD-SiC joint fabricated by SPS joining using pre-sintered Ti_3SiC_2 foil as interlayer at room temperature and high temperatures. Reproduced with permission from Ref. [111], © Elsevier Ltd. 2016.

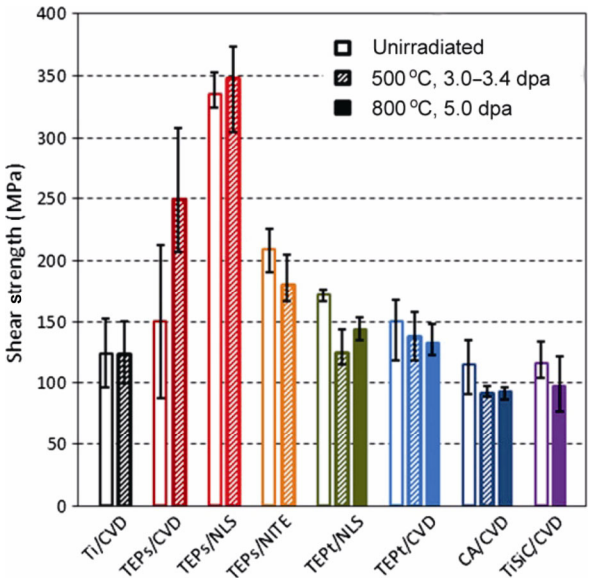

Fig. 11 Torsion shear strength of multiple joints before and after neutron radiation. The Ti, TEPs, TEPt, CA, and TiSiC denote the joining processes using Ti, $SiC+Y_2O_3–Al_2O_3–SiO_2$, $SiC+Y_2O_3–Al_2O_3$, $CaO–Al_2O_3$, and Ti_3SiC_2 as interlayers, respectively. The CVD, NITE, and NLS denote the CVD-SiC, SiC_f/SiC composite fabricated by NITE process and NITE-like sintered SiC, respectively. Reproduced with permission from Ref. [12], © Elsevier B.V. 2013.

joining method for SiC-based materials according to the low interfacial interactions between the interlayers and SiC ceramics or SiC_f/SiC composites, and the resulting joints can be high temperature and irradiation resistant. For instance, Katoh *et al.* [12] reported the pre-irradiated and post-irradiated joint shear strengths and microstructures of CVD-, NLS-, and NITE-SiC joints joined by the TEPs, TEPt, CA, and Ti_3SiC_2 joining processes, and found that some joint materials exhibited significant irradiation-induced microstructural evolution under the more aggressive irradiation conditions (800 ℃, 5 dpa) and that the effect of irradiation on joint strength appeared rather limited (Fig. 11). In particular, both the glass-ceramic joining and reaction forming are greatly promising because of the pressureless process and the obtained relatively high joint strength.

5 Organic interlayer

Joining of SiC-based materials to themselves can be also achieved using preceramic polymers as as-received interlayer by dissolving, coating, crosslinking, and pyrolysis and/or sintering procedures and even further reinfiltration, which process has been rapidly developed in recent two decades since the first fabrication of inorganic ceramic by the organic precursor conversion method [120]. Recently, the preceramic polymers used for joining of SiC-based materials were mainly involved in methyl-hydroxyl-siloxane [121], polysiloxane [19,122,123], polymethylsiloxane [113,124,125], polysilazane [126,127], polymethylsilane [128–130], and allylhydridopolycarbosilane [131,132], as shown in Table 9. Generally, the resulting SiC/SiC joint bending strength values were less than 200 MPa in spite of the formation of interlayer with identical or similar CTE to the SiC-based materials, which were much lower than those obtained by reaction forming/bonding [115–118]. To accelerate the pyrolysis of polymer, and to reduce holes and cracks in the joining interlayer, as well as to initiate chemical reactions between the pyrolysis product and the base material, some metallic and inorganic nanoparticles (such as Ni, Al–12Si, B, SiC, B_4C, low melting point glass and their combinations) as active additives were added in these preceramic polymers for joining of SiC ceramics and SiC_f/SiC composites, resulting in enhancement of joint strength and decrease of joining temperature (Table 9). Moreover, the reinfiltration treatment after joining can remarkably increase the bonding strength of joints. For instance, the 3PB strength of SiC/SiC joint using polysilazane as interlayer was increased from 107.3 to 169.1 MPa after reinfiltration for three cycles, and it was further enhance to ~177 and 256.1 MPa after adding SiC and Ni nanopowders, respectively [126,127].

Table 9 Joining of SiC-based materials using organic (+additives) interlayer: interlayer, heat-treatment process, and joint strength

Joining system	Interlayer	Heat treatment conditions	Joint strength characterization	Maximum average Joint strength	Ref.
SiC_f/SiC//SiC_f/SiC	Methyl-hydroxyl-siloxane (SR350)	1000–1400 ℃, 120 min	Shear strength	~6.5	[121]
SiC_f/SiC//SiC_f/SiC	Methyl-hydroxyl-siloxane+SiC	1000–1400 ℃, 120 min	Shear strength	~7.5	[121]
SiC_f/SiC//SiC_f/SiC	Methyl-hydroxyl-siloxane+Al–12Si	1000–1400 ℃, 60 min	Shear strength	~17.5	[121]
SiC_f/SiC//SiC_f/SiC (3D)	Methyl-hydroxyl-siloxane+Al–12Si	1200 ℃, 60 min (+reinfiltration 4 cycles)	Shear strength	~31.6	[121]
RBSiC/RBSiC	Polysiloxane	1200–1400 ℃, 60–180 min, 0.1–0.4 MPa (+reinfiltration 3 cycles)	Bending strength (3PB)	132.6	[122]
RBSiC/RBSiC	Polysiloxane (YR3184)	1100–1300 ℃, 60 min, 0.02 MPa	Bending strength (3PB)	197	[123]
PLS-SiC/PLS-SiC	Polysiloxane (YR3184)	1100–1300 ℃, 60 min, 0.02 MPa	Bending strength (3PB)	163	[123]
PLS-SiC/PLS-SiC	Polysiloxane (SR355) + Ni	900–1200 ℃, 30 min, 0.4 MPa (+reinfiltration 3 cycles)	Joining strength (3PB) (circular specimen)	74.72	[19]
SiC/SiC	Polymethylsiloxane	300–700 ℃, 60 min	Shear strength (DN)	15.31±1.05	[124]
SiC/SiC	Polymethylsiloxane + epoxy resin + Si–$SnO{\cdot}SiO_2{\cdot}P_2O_5$–Al–$B_4C$	25–1500 ℃, 60 min	Shear strength (DN)	37.28±1.33; 21.58 (800 ℃)	[124]
SiC/SiC	Polyhydridomethylsiloxane+SiC Polyhydridomethylsiloxane +Al–SiC Polyhydridomethylsiloxane + Al–Al_2O_3	1200 ℃, 1–30 MPa 1200 ℃, 1 MPa 1200 ℃, 1 MPa	Shear strength (SL)	~21 ~14.5 ~7	[113]
SiC/SiC	Polyvinylphenylsiloxane	1000–1350 ℃, 120 min	Shear strength	18.9	[125]
RBSiC/RBSiC	Polysilazane	1100–1400 ℃, 0.1–0.2 MPa	Bending strength (3PB)	107.3	[126]
RBSiC/RBSiC	Polysilazane	1100–1400 ℃, 0.1–0.2 MPa (+reinfiltration 3 cycles)	Bending strength (3PB)	169.1	[126]
RBSiC/RBSiC	Polysilazane (SR355) + SiC	1100–1400 ℃ (+reinfiltration 3 cycles)	Bending strength (3PB)	~177	[127]
RBSiC/RBSiC	Polysilazane (SR355) + Ni	1100–1400 ℃ (+reinfiltration 3 cycles)	Bending strength (3PB)	256.1	[127]
SiC/SiC	Polymethylsilane (V-PMS) (modified with D4Vi)	200–1200 ℃,120 min	Shear strength	31.7±2.1	[128]
SiC/SiC	Polymethylsilane (V-PMS) + B_4C	200–1200 ℃, 120 min	Shear strength	50.8±5.6	[128]
SiC/SiC	Polymethylsilane + B_4C-low melting point glass	400–1200 ℃, 120 min	Shear strength	26.2	[129]
SiC/SiC	Polymethylsilane (V-PMS)	800–1200 ℃, 120 min	Shear strength	34.5	[130]
SiC/SiC	Allylhydridopolycarbosilane Allylhydridopolycarbosilane + 30 SiC Polycarbosilane + (40–90)SiC (vol%)	1350 ℃, 120 min (pyrolyzed) + 2150 ℃, 40 min (sintered)	—	—	[131]
SiC/SiC	Allylhydridopolycarbosilane + 30%SiC (vol%)	1250 ℃, 120 min (pyrolyzed) + 2150 ℃, 40 min (sintered)	Bending strength (4PB)	239±69	[132]
SiC/SiC	Allylhydridopolycarbosilane +28%SiC+2%B (vol%)	1250 ℃, 120 min (pyrolyzed) + 2150 ℃, 40 min (sintered)	Bending strength (4PB)	323±16	[132]
CVD-SiC/CVD-SiC	Allylhydridopolycarbosilane (SMP-10)	>1500 ℃, 120 min	Torsion shear strength (THG)	77.7; 81.3 (730 ℃, 4.5 dpa)	[133]

6 Summary

The ceramic joints was mainly characterized mechanically by SLO, 3PB, and 4PB tests at room temperature, so the joint strength characterization should be strengthened by pure shear (such as A4PB, TC, TT, and THG) and mixed stress tests according to practical service stress states at room and elevated temperatures and/or under irradiation.

The joint strengths of SiC-based materials to themselves or metals are closely related to the materials used (involving ceramic and metal components and interlayer materials), interfacial behavior (determined by the materials used and joining process), testing conditions, and loading method, etc. So, to select the two joining objects with the same or similar thermal

physical properties and make appropriate interfacial interactions (such as chemical reaction, elemental diffusion, and adsorption) are the precondition to obtain sound joints.

Joining of SiC-based materials to metals can be performed by using no interlayer and metallic materials as interlayer. However, presently employing glass-ceramic and organic interlayers can only be for homogeneous materials joining of SiC-based materials. Diffusion bonding of monolithic SiC and SiC_f/SiC composites, with high additional pressure, can fabricate high-performance joints, and the TLP bonding, SHS welding, reaction forming/bonding and hot-pressing sinter/reaction joining are the powerful complementary joining techniques for the SiC-based components. The brazing is still the most promising joining technique for fabrication of SiC-based materials/metal complex components.

To develop highly reliable, simple and pressureless (fit to join the large-sized and complex-shaped components) joining process is very urgent for the SiC-based components. Laser-assisted joining process, involving metal brazing and glass-ceramic joining, is greatly promising due to its flexibility and high efficiency. Maybe, a novel joining method for SiC-based materials by in situ formation of MAX phases is worth being further studied based on the recent investigation [31], since the high-performance SiC joints having high strength and good high temperature and irradiation resistances, with promising applications, can be obtained by the simple, pressureless and liquid-based joining process.

Acknowledgements

This work was supported by the National Natural Science Foundation of China (No. 51572112), the National Key R&D Program of China (No. 2017YFB0310400), the 333 Talents Project (No. BRA2017387), Six Talent Peaks Project (No. TD-XCL-004), Innovation/Entrepreneurship Program ([2015]26), and Qing Lan Project ([2016]15) of Jiangsu Province.

References

[1] Zhou XG, Wang HL, Zhao S. Progress of SiC_f/SiC composites for nuclear application. *Adv Ceram* 2016, **37**: 151–167.

[2] Chen MW, Xie WJ, Qiu HP. Recent progress in continuous SiC fiber SiC ceramic matrix composites. *Adv Ceram* 2016, **37**: 393–402.

[3] Liu GW, Qiao GJ, Wang HJ, *et al.* Pressureless brazing of zirconia to stainless steel with Ag–Cu filler metal and TiH_2 powder. *J Eur Ceram Soc* 2008, **28**: 2701–2708.

[4] Liu GW, Qiao GJ, Wang HJ, *et al.* Bonding mechanisms and shear properties of alumina ceramic/stainless steel brazed joint. *J Mater Eng Perform* 2011, **20**: 1563–1568.

[5] Liu HJ, Feng JC, Qian YY. Interface structure and formation mechanism of diffusion-bonded joints of SiC ceramic to TiAl-based alloy. *Scripta Mater* 2000, **43**: 49–53.

[6] Zhang C, Qiao G, Jin Z. Active brazing of pure alumina to Kovar alloy based on the partial transient liquid phase (PTLP) technique with Ni–Ti interlayer. *J Eur Ceram Soc* 2002, **22**: 2181–2186.

[7] Li S, Duan H, Liu S, *et al.* Interdiffusion involved in SHS welding of SiC ceramic to itself and to Ni-based superalloy. *Int J Refract Met H* 2000, **18**: 33–37.

[8] Uday MB, Ahmad Fauzi MN, Zuhailawati H, *et al.* Effect of welding speed on mechanical strength of friction welded joint of YSZ-alumina composite and 6061 aluminum alloy. *Mat Sci Eng A* 2011, **528**: 4753–4760.

[9] Döhler F, Zscheckel T, Kasch S, *et al.* A glass in the $CaO/MgO/Al_2O_3/SiO_2$ system for the rapid laser sealing of alumina. *Ceram Int* 2017, **43**: 4302–4308

[10] Singh M. A reaction forming method for joining of silicon carbide-based ceramics. *Scripta Mater* 1997, **37**: 1151–1154.

[11] Krenkel W, Henke T, Mason N. In-situ joined CMC components. *Key Eng Mater* 1996, **127**: 313–320.

[12] Katoh Y, Snead LL, Cheng T, *et al.* Radiation-tolerant joining technologies for silicon carbide ceramics and composites. *J Nucl Mater* 2014, **448**: 497–511.

[13] Ferraris M, Salvo M, Casalegno V, *et al.* Torsion tests on AV119 epoxy-joined SiC. *Int J Appl Ceram Technol* 2012, **9**: 795–807.

[14] Ferraris M, Ventrella A, Salvo M, *et al.* Shear strength measurement of AV119 epoxy-joined SiC by different torsion tests. *Int J Appl Ceram Technol* 2014, **11**: 394–401.

[15] Zhang X, Liu G, Tao J, *et al.* Brazing of WC–8Co cemented carbide to steel using Cu–Ni–Al alloys as filler metal: Microstructures and joint mechanical behavior. *J Mater Sci Technol* 2018, **34**: 1180–1188.

[16] Zhang X, Huang Z, Liu G, *et al.* Wetting and brazing of Ni-coated WC-8Co cemented carbide using the Cu–19Ni–5Al alloy as filler metal: Microstructural evolution and joint mechanical properties. *J Mater Res* 2018, **33**: 1671–1680.

[17] Salvo M, Rizzo S, Casalegno V, *et al.* Shear and bending strength of SiC/SiC joined by a modified commercial adhesive. *Int J Appl Ceram Technol* 2012, **9**: 778–785.

[18] Ferraris M, Salvo M, Casalegno V, *et al.* Joining of machined SiC/SiC composites for thermonuclear fusion

reactors. *J Nucl Mater* 2008, **375**: 410–415.

[19] Li SJ, Liu WH, Lu YH, *et al.* Joining of pressureless sintered SiC using polysiloxane SR355 with active additive Ni nanopowder. *Acta Mater Compos Sin* 2008, **25**: 72–76.

[20] Dong H, Li S, Teng Y, *et al.* Joining of SiC ceramic-based materials with ternary carbide Ti_3SiC_2. *Mat Sci Eng B* 2011, **176**: 60–64.

[21] Li SJ, Zhou Y, Duan HP, *et al.* Joining of SiC ceramic to Ni-based superalloy with functionally gradient material fillers and a tungsten intermediate layer. *J Mater Sci* 2003, **38**: 4065–4070.

[22] Dong HY, Li SJ, He YH. Joining of reaction bonded SiC ceramic using Ti_3SiC_2 powder as filler. *Chin J Nonfer Metal* 2005, **15**: 1051–1056.

[23] Aroshas R, Rosenthal I, Stern A, *et al.* Silicon carbide diffusion bonding by spark plasma sintering. *Mater Manuf Process* 2015, **30**: 122–126.

[24] Grasso S, Tatarko P, Rizzo S, *et al.* Joining of β-SiC by spark plasma sintering. *J Eur Ceram Soc* 2014, **34**: 1681–1686.

[25] Okuni T, Miyamoto Y, Abe H, *et al.* Joining of silicon carbide and graphite by spark plasma sintering. *Ceram Int* 2014, **40**: 1359–1363.

[26] Kishimoto H, Shibayama T, Abe T, *et al.* Diffusion bonding technology of tungsten and SiC/SiC composites for nuclear applications. *IOP Conf Ser: Mater Sci* 2011, **18**: 162015

[27] Kishimoto H, Shibayama T, Shimoda K. Microstructural and mechanical characterization of W/SiC bonding for structural material in fusion. *J Nucl Mater* 2011, **417**: 387–390.

[28] Matsuo G, Shibayama T, Kishimoto H, *et al.* Micro-chemical analysis of diffusion bonded W–SiC joint. *J Nucl Mater* 2011, **417**: 391–394.

[29] Zhong Z, Hinoki T, Kohyama A. Microstructure and mechanical strength of diffusion bonded joints between silicon carbide and F82H steel. *J Nucl Mater* 2011, **417**: 395–399.

[30] Pan H, Itoh I, Matsubara M. Mechanical properties of diffusion bonding joint of SiC and Al–Sn alloys at elevated temperatures. *Mater Trans* 2001, **42**: 2543–2547.

[31] Sozhamannan GG, Prabu SB. Influence of interface compounds on interface bonding characteristics of aluminium and silicon carbide. *Mater Charact* 2009, **60**: 986–990.

[32] Sozhamannan GG, Balasivanandha Prabu S. Evaluation of interface bonding strength of aluminum/silicon carbide. *Int J Adv Manuf Technol* 2009, **44**: 385–388.

[33] Valenza F, Gambaro S, Muolo ML, *et al.* Wetting of SiC by Al–Ti alloys and joining by in-situ formation of interfacial $Ti_3Si(Al)C_2$. *J Eur Ceram Soc* 2018, **38**: 3727–3734.

[34] Zhang Z, Huang J, Zhang H, *et al.* Microstructures of Si/SiC ceramic and invar alloy brazing joint. *Rare Metal Mater Eng* 2009, **38**: 493–496.

[35] Zhao HT, Huang JH, Zhang H, *et al.* Vacuum brazing of Si/SiC ceramic and low expansion titanium alloy by using Cu–Ti fillers. *Rare Metal Mater Eng* 2007, **36**: 2184–2188.

[36] Riccardi B, Nannetti CA, Woltersdorf J, *et al.* Brazing of SiC and SiC_f/SiC composites performed with 84Si–16Ti eutectic alloy: Microstructure and strength. *J Mater Sci* 2002, **37**: 5029–5039.

[37] Riccardi B, Nannetti CA, Woltersdorf J, *et al.* Joining of SiC based ceramics and composites with Si–16Ti and Si–18Cr eutectic alloys. *Int J Mater Prod Technol* 2004, **20**: 440–451.

[38] Li JK, Liu L, Liu X. Joining of SiC ceramic by 22Ti–78Si high-temperature eutectic brazing alloy. *J Inorg Mater* 2011, **26**: 1314–1318.

[39] Nagatsuka K, Sechi Y, Nakata K. Dissimilar joint characteristics of SiC and WC–Co alloy by laser brazing. *J Phys: Conf Ser* 2012, **379**: 012047.

[40] Liu HJ, Feng JC, Qian YY. Microstructure and strength of the SiC/TiAl joint brazed with Ag–Cu–Ti filler metal. *J Mater Sci Lett* 2000, **19**: 1241–1242.

[41] Liu Y, Huang ZR, Liu XJ. Joining of sintered silicon carbide using ternary Ag–Cu–Ti active brazing alloy. *Ceram Int* 2009, **35**: 3479–3484.

[42] Prakash P, Mohandas T, Raju PD. Microstructural characterization of SiC ceramic and SiC-metal active metal brazed joints. *Scripta Mater* 2005, **52**: 1169–1173.

[43] Liu Y, Zhu YZ, Yang Y, *et al.* Microstructure of reaction layer and its effect on the joining strength of SiC/SiC joints brazed using Ag–Cu–In–Ti alloy. *J Adv Ceram* 2014, **3**: 71–75.

[44] Moszner F, Mata-Osoro G, Chiodi M, *et al.* Mechanical behavior of SiC joints brazed using an active Ag–Cu–In–Ti braze at elevated temperatures. *Int J Appl Ceram Technol* 2017, **14**: 703–711.

[45] Lv H, Kang ZJ, Chu JX, *et al.* Microstructure and strength of SiC/Nb joint with Cu based brazing filler metal. *Trans Chin Weld Inst* 2005, **26**: 29–31.

[46] Südmeyer I, Hettesheimer T, Rohde M. On the shear strength of laser brazed SiC–steel joints: Effects of braze metal fillers and surface patterning. *Ceram Int* 2010, **36**: 1083–1090.

[47] Tian WB, Sun ZM, Zhang P, *et al.* Brazing of silicon carbide ceramics with Ni–Si–Ti powder mixtures. *J Aust Ceram Soc* 2017, **53**: 511–516.

[48] Xiong HP, Mao W, Xie YH, *et al.* Control of interfacial reactions and strength of the SiC/SiC joints brazed with newly-developed Co-based brazing alloy. *J Mater Res* 2007, **22**: 2727–2736.

[49] Xiong HP, Mao W, Xie YH, *et al.* Brazing of SiC to a wrought nickel-based superalloy using CoFeNi(Si,B)CrTi filler metal. *Mater Lett* 2007, **61**: 4662–4665.

[50] Chen XG, Xie RS, Lai ZW, *et al.* Interfacial structure and

formation mechanism of ultrasonic-assisted brazed joint of SiC ceramics with Al–12Si filler metals in air. *J Mater Sci Technol* 2017, **33**: 492–498.

[51] Chen XG, Yan JC, Ren SC, *et al.* Ultrasonic-assisted brazing of SiC ceramic to Ti–6Al–4V alloy using a novel AlSnSiZnMg filler metal. *Mater Lett* 2013, **105**: 120–123.

[52] Chen XG, Yan JC, Ren SC, *et al.* Microstructure, mechanical properties, and bonding mechanism of ultrasonic-assisted brazed joints of SiC ceramics with ZnAlMg filler metals in air. *Ceram Int* 2014, **40**: 683–689.

[53] Koltsov A, Hodaj F, Eustathopoulos N. Brazing of AlN to SiC by a Pr silicide: Physicochemical aspects. *Mat Sci Eng A* 2008, **495**: 259–264,

[54] Riccardi B, Nannetti CA, Petrisor T, *et al.* Issues of low activation brazing of SiC_f/SiC composites by using alloys without free silicon. *J Nucl Mater* 2004, **329**: 562–566.

[55] Li HX, Wang ZQ, Zhong ZH, *et al.* Micro-alloying effects of yttrium on the microstructure and strength of silicon carbide joint brazed with chromium–silicon eutectic alloy. *J Alloys Compd* 2018, **738**: 354–362.

[56] Li WW, Chen B, Xiong HP, *et al.* Brazing SiC matrix composites using Co–Ni–Nb–V alloy. *Weld World* 2017, **61**: 839–846.

[57] Mao YW, Li SJ, Han WB. Joining of SiC by high temperature brazing with Ni–51Cr filler. *Rare Metal Mater Eng* 2006, **35**: 312–315.

[58] Mao YW, Li SJ, Han WB. Joining of recrystallized SiC ceramic using Ni–Cr–Nb powders as filler. *Rare Metal Mater Eng* 2009, **38**: 276–279.

[59] Chen B, Xiong HP, Mao W, *et al.* Microstructures and property of SiC/SiC joints brazed with PdNi–Cr–V brazing filler. *Acta Metall Sin* 2007, **43**: 1181–1185.

[60] Wang Q, Li QH, Sun DL, *et al.* Microstructure and mechanical properties of SiC/Ti diffusion bonding joints under electric field. *Rare Metal Mater Eng* 2016, **45**: 1749–1754.

[61] Jung YI, Park JH, Kim HG, *et al.* Effect of Ti and Si interlayer materials on the joining of SiC ceramics. *Nucl Eng Technol* 2016, **48**: 1009–1014.

[62] Cockeram BV. Flexural strength and shear strength of silicon carbide to silicon carbide joints fabricated by a molybdenum diffusion bonding technique. *J Am Ceram Soc* 2005, **88**: 1892–1899.

[63] Kim JH, Kim DS, Lim ST, *et al.* Interfacial microstructure of diffusion-bonded SiC and Re with Ti Interlayer. *J Alloys Compd* 2017, **701**: 316–320.

[64] Kurumada A, Imamura Y, Tomota Y, *et al.* Evaluation of the integrity of divertor models of tungsten or SiC/SiC composites joined with copper. *J Nucl Mater* 2003, **313**: 245–249.

[65] Ji XQ, Li SJ, Ma TY, *et al.* Joining of SiC ceramic to Ni-based superalloy with Zr/Nb multiple interlayers. *J Chin Ceram Soc* 2002, **30**: 305–310.

[66] Tenyama K, Maeda M, Shibayanagi T, *et al.* Interfacial microstructure of silicon carbide and titanium aluminide joints produced by solid-state diffusion bonding. *Mater Trans* 2004, **45**: 2734–2739.

[67] Liu HJ, Feng JC. Diffusion bonding of SiC ceramic to TiAl-based alloy. *J Mater Sci Lett* 2001, **20**: 815–817.

[68] Feng JC, Liu HJ, Naka M, *et al.* Interface structure and formation mechanism of diffusion-bonded SiC/Ni–Cr joint. *J Mater Sci Lett* 2001, **20**: 301–302.

[69] Feng JC, Liu HJ, Naka M, *et al.* Reaction products and growth kinetics during diffusion bonding of SiC ceramic to Ni–Cr alloy. *Mater Sci Technol* 2003, **19**: 137–142.

[70] Li JQ, Zhu GM, Xiao P. Joining reaction-bonded silicon carbide using Inconel 600 superalloy. *J Mater Sci Lett* 2003, **22**: 759–761.

[71] Zhong ZH, Hinoki T, Kohyama A, *et al.* Joining of silicon carbide to ferritic stainless steel using a W–Pd–Ni interlayer for high-temperature applications. *Int J Appl Ceram Technol* 2010, **7**: 338–347.

[72] Li HX, Zhong ZH, Zhang HB, *et al.* Microstructure characteristic and its influence on the strength of SiC ceramic joints diffusion bonded by spark plasma sintering. *Ceram Int* 2018, **44**: 3937–3946.

[73] Liu GW, Muolo ML, Valenza F, *et al.* Survey on wetting of SiC by molten metals. *Ceram Int* 2010, **36**: 1177–1188.

[74] Hynes NRJ, Velu PS, Kumar R, *et al.* Investigate the influence of bonding temperature in transient liquid phase bonding of SiC and copper. *Ceram Int* 2017, **43**: 7762–7767.

[75] Liu GW, Valenza F, Muolo ML, *et al.* SiC/SiC and SiC/Kovar joining by Ni–Si and Mo interlayers. *J Mater Sci* 2010, **45**: 4299–4307.

[76] Zhang JJ, Li SJ, Duan HP, *et al.* Effects of technological parameters on the joining strength of SiC ceramic by hot pressing reaction welding. *Rare Metal Mater Eng* 2003, **32**: 542–545.

[77] Duan HP, Li SJ, Zhang YG, *et al.* Investigation on welding process of SiC ceramic with Ni-based superalloy using Gleeble 1500 thermo-mechanical testing machine. *Chin J Rare Metal* 1999, **23**: 326–329.

[78] Lin YC, McGinn PJ, Mukasyan AS. High temperature rapid reactive joining of dissimilar materials: Silicon carbide to an aluminum alloy. *J Eur Ceram Soc* 2012, **32**: 3809–3818.

[79] Gianchandani PK, Casalegno V, Smeacetto F, *et al.* Pressure-less joining of C/SiC and SiC/SiC by a $MoSi_2$/Si composite. *Int J Appl Ceram Technol* 2017, **14**: 305–312.

[80] Lin GB, Huang JH, Zhang JG, *et al.* Microstructure of reactive composite brazing joints of SiC ceramics and Ti alloy by using Ag–Cu–Ti–(Ti+C) as bonding material. *Chin J Nonfer Metal* 2005, **15**: 1326–1331.

[81] Dai XY, Cao J, Chen Z, *et al.* Brazing SiC ceramic using novel B_4C reinforced Ag–Cu–Ti composite filler. *Ceram Int* 2016, **42**: 6319–6328.

[82] Dai XY, Cao J, Tian YT, *et al.* Effect of holding time on microstructure and mechanical properties of SiC/SiC joints brazed by Ag–Cu–Ti+B_4C composite filler. *Mater Charact* 2016, **118**: 294–301.

[83] Ma Q, Li ZR, Wang ZY, *et al.* Relieving residual stress in brazed joint between SiC and Nb using a 3D-SiO_2-fiber ceramic interlayer. *Vacuum* 2018, **149**: 93–95.

[84] Liu Y, Qi Q, Zhu YZ, *et al.* Microstructure and joining strength evaluation of SiC/SiC joints brazed with SiCp/Ag–Cu–Ti hybrid tapes. *J Adhes Sci Technol* 2015, **29**: 1563–1571.

[85] Mao YW, Li SJ, Yan LS. Joining of SiC ceramic to graphite using Ni–Cr–SiC powders as filler. *Mat Sci Eng A* 2008, **491**: 304–308.

[86] Tian WB, Kita H, Kondo N, *et al.* Effect of composition and joining parameters on microstructure and mechanical properties of silicon carbide joints. *J Ceram Soc Jpn* 2010, **118**: 799–804.

[87] Tian WB, Kita H, Hyuga H, *et al.* Reaction joining of SiC ceramics using TiB_2-based composites. *J Eur Ceram Soc* 2010, **30**: 3203–3208.

[88] Tian WB, Kita H, Hyuga H, *et al*. Joining of SiC by Al infiltrated TiC tape: Effect of joining parameters on the microstructure and mechanical properties. *J Eur Ceram Soc* 2012, **32**: 149–156.

[89] Rosa R, Veronesi P, Han S, *et al.* Microwave assisted combustion synthesis in the system Ti–Si–C for the joining of SiC: Experimental and numerical simulation results. *J Eur Ceram Soc* 2013, **33**: 1707–1719.

[90] Katoh Y, Kotani M, Kohyama A, *et al.* Microstructure and mechanical properties of low-activation glass-ceramic joining and coating for SiC/SiC composites. *J Nucl Mater* 2000, **283**: 1262–1266.

[91] Ferraris M, Salvo M, Casalegno V, *et al.* Joining of SiC-based materials for nuclear energy applications. *J Nuc Mater* 2011, **417**: 379–382.

[92] Ferraris M, Salvo M, Rizzo S, *et al.* Torsional shear strength of silicon carbide components pressurelessly joined by a glass-ceramic. *Int J Appl Ceram Technol* 2012, **9**: 786–794.

[93] Ferraris M, Ventrella A, Salvo M, *et al.* Torsional shear strength tests for glass-ceramic joined silicon carbide. *Int J Appl Ceram Technol* 2015, **12**: 693–699.

[94] Lippmann W, Knorr J, Wolf R, *et al.* Laser joining of silicon carbide—a new technology for ultra-high temperature resistant joints. *Nucl Eng Des* 2004, **231**: 151–161.

[95] Herrmann M, Lippmann W, Hurtado A. High-temperature stability of laser-joined silicon carbide components. *J Nucl Mater* 2013, **443**: 458–466.

[96] Ferraris M, Casalegno V, Rizzo S, *et al.* Effects of neutron irradiation on glass ceramics as pressure-less joining materials for SiC based components for nuclear applications. *J Nucl Mater* 2012, **429**: 166–172.

[97] Schaafhausen S, Börner FD, Chand T, *et al.* Corrosion of laser joined silicon carbide in gasification environment. *Adv Appl Ceram* 2015, **114**: 350–360.

[98] Herrmann M, Lippmann W, Hurtado A. Y_2O_3–Al_2O_3–SiO_2-based glass-ceramic fillers for the laser-supported joining of SiC. *J Eur Ceram Soc* 2014, **13**:1935–1948.

[99] Fan SW, Liu JL, Ma X, *et al.* Microstructure and properties of SiC_f/SiC joint brazed by Y–Al–Si–O glass. *Ceram Int* 2018, **44**: 8656–8663.

[100] Ahmad S, Herrmann M, Mahmoud MM, *et al.* Application of Nd_2O_3–Al_2O_3–SiO_2 glass solder for joining of silicon carbide components. *J Eur Ceram Soc* 2016, **36**: 1559–1569.

[101] Herrmann M, Ahmad S, Lippmann W, *et al.* Rare earth (RE: Nd, Dy, Ho, Y, Yb, and Sc) aluminosilicates for joining silicon carbide components. *Int J Appl Ceram Technol* 2017, **14**: 675–691.

[102] Luo ZH, Jiang DL, Zhang JX, *et al.* Investigation of interfacial bonding between Na_2O–B_2O_3–SiO_2 solder and silicon carbide Substrate. *Sci Technol Weld Joining* 2011, **16**: 592–596.

[103] Luo ZH, Jiang DL, Zhang JX, *et al.* Joining of sintered silicon carbide ceramics using sodium borosilicate glass as the solder. *Int J Appl Ceram Technol* 2012, **9**: 742–750.

[104] Luo ZH, Jiang DL, Zhang JX, *et al.* Thermal shock behavior of the SiC–SiC joints joined with Na_2O–B_2O_3–SiO_2 glass solder. *J Inorg Mater* 2012, **27**: 234–238.

[105] Jung HC, Park YH, Park JS, *et al.* R&D of joining technology for SiC components with channel. *J Nucl Mater* 2009, **386–388**: 847–851.

[106] Jung HC, Hinoki T, Katoh Y, *et al.* Development of a shear strength test method for NITE–SiC joining material. *J Nucl Mater* 2011, **417**: 383–386.

[107] Yoon HK, Jung HC, Hinoki T, *et al.* Characteristics of shear strength for joined SiC–SiC ceramics. *Trans Korean Soc Mech Eng A* 2014, **38**: 483–487.

[108] Tian WB, Kita H, Hyuga H, *et al.* Joining of SiC by tape-cast SiC–Al_2O_3–Y_2O_3 interlayer. *Key Eng Mater* 2011, **484**: 26–31.

[109] Dong HY, Yu YD, Jin XL, *et al.* Microstructure and mechanical properties of SiC–SiC joints joined by spark plasma sintering. *Ceram Int* 2016, **42**: 14463–14468.

[110] Zhou XB, Han YH, Shen XF, *et al.* Fast joining SiC ceramics with Ti_3SiC_2 tape film by electric field-assisted sintering technology. *J Nucl Mater* 2015, **466**: 322–327.

[111] Tatarko P, Chlup Z, Mahajan A, *et al.* High temperature properties of the monolithic CVD β-SiC materials joined with a pre-sintered MAX phase Ti_3SiC_2 interlayer via solid-state diffusion bonding. *J Eur Ceram Soc* 2017, **37**: 1205–1216.

[112] Henager CH, Kurtz RJ. Low-activation joining of SiC/SiC composites for fusion applications. *J Nucl Mater* 2011, **417**: 375–378.

[113] Henager CH, Shin Y, Bium Y, *et al.* Coatings and joining for SiC and SiC-composites for nuclear energy systems. *J Nucl Mater* 2007, **367**: 1139–1143.

[114] Yu YD, Dong HY, Ma BL, *et al.* Effect of different filler

materials on the microstructure and mechanical properties of SiC–SiC joints joined by spark plasma sintering. *J Alloys Compd* 2017, **708**: 373–379.

[115] Zhang AF, Chen YC, Chen ZQ, *et al.* Joining of silicon carbide ceramic for optical application by reaction bonded technology. In Proceedings of the 5th International Symposium on Advanced Optical Manufacturing and Testing Technologies: Large Mirrors and Telescopes. International Society for Optics and Photonics, 2010, **7654**: 765410.

[116] Tian WB, Kita H, Hyuga H, *et al.* Joining of SiC with Si infiltrated tape-cast TiB_2–C interlayer: Effect of interlayer composition and thickness on the microstructure and mechanical properties. *Mat Sci Eng A* 2011, **530**: 580–584.

[117] Wu QD, Sun F, Ji XL, *et al.* Joining of pure carbide reaction-bonded silicon carbide ceramics. *Rare Metal Mater Eng* 2005, **34**: 515–518.

[118] Wu QD, Sun F, Tian TY, *et al.* Effect of welding solder properties on joining of reaction-bonded silicon carbide. *J Chin Ceram Soc* 2006, **34**: 796–800.

[119] Lewinsohn CA, Singh M, Shibayama T, *et al.* Joining of silicon carbide composites for fusion energy applications. *J Nucl Mater* 2000, **283–287**: 1258–1261.

[120] Liu HL, Li SJ. Joining of SiC and SiC-based composites using preceramic ploymers. *J Chin Ceram Soc* 2004, **32**: 1246–1251.

[121] Colombo P, Riccardi B, Donato A, *et al.* Joining of SiC/SiC_f ceramic matrix composites for fusion reactor blanket applications. *J Nucl Mater* 2000, **278**: 127–135.

[122] Liu HL, Li SJ, Chen ZJ. Joining of reaction-bonded silicon carbide using a polysiloxane. *Rare Metal Mater Eng* 2006, **35**: 134–137.

[123] Yuan XK, Chen S, Zhang XH, *et al.* Joining SiC ceramics with silicon resin YR3184. *Ceram Int* 2009, **35**: 3241–3245.

[124] Tang B, Wang MC, Liu RM, *et al.* A heat-resistant preceramic polymer with broad working temperature range for silicon carbide joining. *J Eur Ceram Soc* 2018, **38**: 67–74.

[125] Zhou BF, Feng KQ, Zhou HL, *et al.* Joining of SiC ceramic by using the liquid polyvinylphenylsiloxane. *Adv Appl Ceram* 2018, **117**: 212–216.

[126] Liu HL, Li SJ, Zhang T, *et al.* Joining of reaction-bonded silicon carbide using SiC/Si_3N_4 preceramic polymer. *Rare Metal Mater Eng* 2005, **34**: 1469–1472.

[127] Liu HL, Li SJ, Li XG. Effect of nickel nanopowders addition on joining property of silicon carbide to itself by polysilazane. *Rare Metal Mater Eng* 2005, **34**: 1905–1908.

[128] Wang XZ, Wang J, Wang H. Synthesis of a novel preceramic polymer (V-PMS) and its performance in heat-resistant organic adhesives for joining SiC ceramic. *J Eur Ceram Soc* 2012, **32**: 3415–3422.

[129] Wang XZ, Wang J, Wang H. Preparation of high-temperature organic adhesives and their performance for joining SiC ceramic. *Ceram Int* 2013, **39**: 1365–1370.

[130] Wang XZ, Wang J, Wang H. Joining of SiC ceramics via a novel liquid preceramic polymer (V-PMS). *Ceram Int* 2015, **41**: 7283–7288.

[131] Zheng J, Beckman SP, Gray JN, *et al.* X-ray tomography study on green state joining of silicon carbide using polymer precursors. *J Am Ceram Soc* 2001, **84**: 1961–1967.

[132] Zheng J, Akinc M. Green state joining of SiC without applied pressure. *J Am Ceram Soc* 2001, **84**: 2479–2483.

[133] Khalifa HE, Koyanagi T, Jacobsen GM, *et al.* Radiation stable, hybrid, chemical vapor infiltration/preceramic polymer joining of silicon carbide components. *J Nucl Mater* 2017, **487**: 91–95.